MOLECULAR AND CELLULAR BIOLOGY, June 2010, p. 2651–2667 Vol. 30, No. 11
0270-7306/10/$12.00 doi:10.1128/MCB.01340-09

skn-1-Dependent and -Independent Regulation of *aip-1* Expression following Metabolic Stress in *Caenorhabditis elegans*▽

Annabel A. Ferguson, Mitchell G. Springer, and Alfred L. Fisher*

University of Pittsburgh, Department of Medicine, Division of Geriatric Medicine, 3471 5th Ave., Suite 500, Pittsburgh, Pennsylvania 15260

Received 5 October 2009/Returned for modification 14 November 2009/Accepted 21 March 2010

Maintenance of a stable, properly folded, and catalytically active proteome is a major challenge to organisms in the face of multiple internal and external stresses which damage proteins and lead to protein misfolding. Here we show that internal metabolic stress produced by reactive intermediates resulting from tyrosine degradation triggers the expression of the *aip-1* gene, which is critical in responses to the environmental toxin arsenic and the clearance of unstable polyglutamine and Aβ proteins. *aip-1* acts via binding to the proteosome and enhancing proteosomal function. We find that full induction of *aip-1* depends on the oxidative-stress-responsive *skn-1* transcription factor but significant induction still occurs without *skn-1*. Importantly, activation of *skn-1* with *wdr-23*(*RNAi*), which dramatically induces the expression of other *skn-1* target genes, produces a minimal increase in *aip-1* expression. This suggests that the previously demonstrated specificity in *aip-1*/AIRAP induction could reflect the actions of multiple synergistic activators, such as the heat shock factor homolog *hsf-1*, which we also find is required for full induction. These may be triggered by proteosome dysfunction, as we find that this event links the multiple inducers of *aip-1*. Together, our results show that cell stress triggers *aip-1* expression by both *skn-1*-dependent and -independent pathways.

In all eukaryotes, tyrosine is converted into energy via a five-step metabolic pathway (Fig. 1) (44). Impaired tyrosine degradation is observed in hereditary type I tyrosinemia, where mutations affecting fumarylacetoacetate hydrolase (FAH), which catalyzes the final step in the pathway, produce elevations in highly reactive tyrosine metabolites such as fumarylacetoacetate and maleylacetoacetate, which damage proteins and DNA (4, 6, 7, 13, 15, 17, 18, 21, 27–29, 34, 36, 39, 52, 59). We have shown that hereditary type I tyrosinemia can be modeled in *Caenorhabditis elegans* through treatment of worms with interfering RNA against the FAH homolog *fah-1* (18). The resulting impairment in tyrosine degradation has dramatic effects on treated worms, including a shortened life span, destruction of the intestine, and decreased fertility. Further, RNA interference (RNAi) treatment leads to the activation of several cell stress responses, including those for oxidative and endoplasmic reticulum (ER) stress, in worms (18). Impaired tyrosine degradation also leads to accelerated aggregation of an aggregation-prone polyglutamine repeat protein in worms, but the mechanism leading to this increase is unclear (49).

The *aip-1*/AIRAP (arsenic-inducible RNA-associated protein) proteins were initially identified as part of the response to the environmental toxin arsenic (56). Arsenic produces multiple types of cell stress, including ER stress, oxidative stress, and protein misfolding (56). Following exposure to arsenic, the *aip-1*/AIRAP proteins are induced at the transcriptional level (56). These proteins bind to the 19S regulatory cap of the proteosome and augment its ability to clear damaged proteins by enhancing substrate access to the catalytic core (57). In addition, *aip-1* also is constitutively expressed in worms at a low level, and this expression is essential in *C. elegans* to maintain proteostasis in animals expressing an aggregation-prone polyglutamine repeat protein or Aβ peptide and to ensure normal worm longevity (23, 64). A related mammalian protein, AIRAPL, also shows constitutive expression, is likely prenylated via a C-terminal CAAX motif, and is associated with the ER in the absence of cell stress (64). In contrast, AIRAP is diffusely expressed in the cytoplasm following induction (56, 64). Together, this suggests that AIRAP is primarily regulated at the transcriptional level whereas AIRAPL is regulated at the posttranslational level by stress (64). The *aip-1* gene shares properties of both in that it is both constitutively expressed and induced by cell stress, and additionally, *aip-1* has a C-terminal CAAX motif which is required for function (64). Important unanswered questions with regard to *aip-1*/AIRAP include identifying the spectrum of inducers, learning whether stressors other than unstable proteins or xenobiotics can stimulate expression, and determining how inducers are identified by cells and activate *aip-1*/AIRAP expression.

Known inducers of *aip-1*/AIRAP expression include arsenic, overexpression of an aggregation prone Aβ peptide in worm muscle, *tert*-butyl peroxide, juglone, and heat shock (23, 25, 50, 53, 56). Arsenic triggers the expression of *aip-1* in worms via the activation of the *skn-1* transcription factor (57). *skn-1* is a bZIP protein which coordinates responses to oxidative stress in worms (2, 3, 11, 26, 30). Since arsenic produces oxidative stress, it is not unexpected that *skn-1* is involved in the control of *aip-1*, but it is not clear if *skn-1* is the sole transcription factor involved in the control of *aip-1* expression. It is possible that misfolded proteins could also act through *skn-1*, because proteosomal dysfunction has been shown to be an activator of *skn-1* nuclear translocation and target gene expression (30). Alternatively, *aip-1* could be induced independently of *skn-1*,

* Corresponding author. Mailing address: University of Pittsburgh, Department of Medicine, Division of Geriatric Medicine, 3471 5th Ave., Suite 500, Pittsburgh, PA 15260. Phone: (412) 383-5892. Fax: (412) 692-2370. E-mail: fishera@dom.pitt.edu.
▽ Published ahead of print on 29 March 2010.

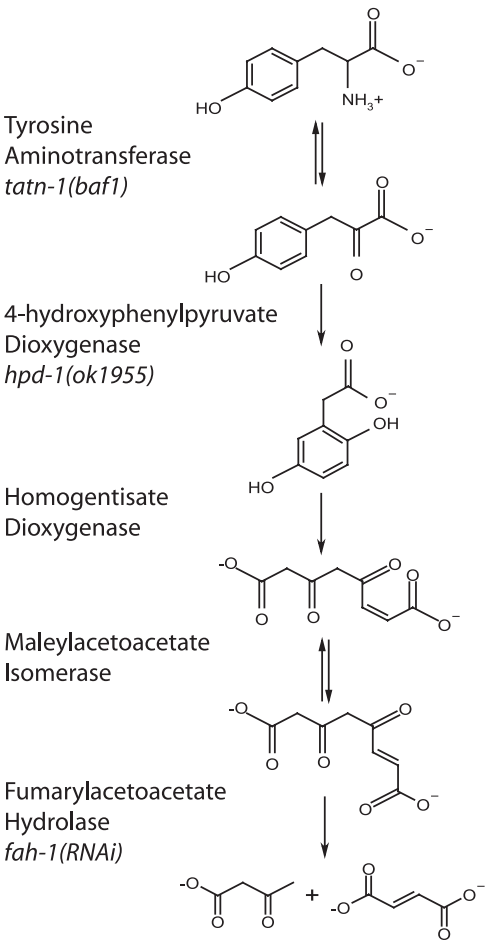

FIG. 1. Tyrosine is degraded via a five-step metabolic pathway. Shown are the chemical structures of the intermediates and enzymes involved in catalyzing each step. Also indicated are the locations of the *tatn-1*(*baf1*) and *hpd-1*(*ok1955*) mutations and *fah-1*(*RNAi*) used to manipulate levels of the reactive metabolites maleylacetoacetate and fumarylacetoacetate.

as suggested in a recent microarray study using *tert*-butyl peroxide (50). Both *hsf-1* and the zinc finger protein-encoding gene *slr-2* have been shown to be required for *aip-1* expression following heat shock, so *hsf-1* or *slr-2* could also be involved in the effects of stressors on *aip-1* expression (25, 35).

In this work, we explore the *in vivo* effects of tyrosine metabolites on cell stress responses. The overlap between the effects produced by arsenic exposure and impaired tyrosine degradation with regard to cell stresses led to the hypothesis that tyrosine metabolites represent endogenous activators of *aip-1* in *C. elegans*. We test this hypothesis and find that these metabolites are endogenous triggers for *aip-1* expression. Hence, while *aip-1* can respond to external stressors, these internal stressors may represent a more common trigger for the pathway. We further find that a pathway involving the oxidative-stress-sensitive transcription factor *skn-1* is required for the full expression of *aip-1*. But in contrast to other *skn-1* target genes studied, the activation of *aip-1* can still occur in the absence of *skn-1*, which suggests a degree of redundancy in the regulation mechanism (2, 3, 26, 30). Further, the activation of *skn-1* alone is unable to induce *aip-1* expression, which is consistent with a necessary role for additional regulators. One of these regulators could be the worm heat shock factor homolog *hsf-1*, which has been shown to regulate *aip-1* expression following heat shock and we find is also required for full expression of *aip-1* in response to metabolic stress (25). Finally, while the exact stimulus for *aip-1* expression is unknown, we present evidence that impaired proteosome function could be a common inducer of the pathway, as we find that *aip-1* is induced by multiple stimuli, including RNAi against heat shock proteins and proteosomal subunits or the chemical juglone, which would be expected to increase cellular levels of damaged proteins. Consistently, we observe enhanced polyglutamine repeat protein aggregation in worms treated with *fah-1*(*RNAi*), as well as a dramatic increase in polyubiquitinated proteins. Together, our results demonstrate that both *skn-1*-dependent and -independent pathways contribute to the control of *aip-1* expression following metabolic stress.

MATERIALS AND METHODS

Strains. SJ4003 (*aip-1p*:*GFP*) was a gift of David Ron (NYU, New York, NY) (56). AM140 (*rmIs132*), CL2166 {*dvIs19*[*pAF15*(*gst-4*::*GFP*::*NLS*)]}, DP38 [*unc-119*(*ed3*)], FK171 [*mek-1*(*ks54*)], KU4 [*sek-1*(*km4*)], KU25 [*pmk-1*(*km25*)], TJ1060 [*spe-9*(*hc88*), *fer-15*(*b26*)], and VC1539 [*hpd-1*(*ok1955*)] were obtained from the Caenorhabditis Genetics Center, which is funded by the NIH National Center for Research Resources. LG335 {*skn-1*(*zu135*)/*nT1*[*qIs51*]} was a gift of Nicholas Bishop and Leonard Guarente (8). LG335 was crossed with SJ4003 to generate ALF127 {*skn-1*(*zu135*)/*nT1*[*qIs51*] *aip-1p*:*GFP*}. VC1539 was outcrossed three times with N2 to generate ALF114. ALF103 [*tatn-1*(*baf1*)] was described previously (18). Strains carrying *aip-1p*:*GFP* or *Q35*:*YFP* and *hpd-1*(*ok1955*), *tatn-1*(*baf1*), *mek-1*(*ks54*), *sek-1*(*km4*), and *pmk-1*(*km25*) were created by standard genetic crosses. The presence of *hpd-1*(*ok1955*), *mek-1*(*ks54*), *sek-1*(*km4*), and *pmk-1*(*km25*) was verified by single-worm PCR using deletion-specific oligonucleotides (sequences are available upon request). *tatn-1*(*baf1*) was verified by single-worm PCR, followed by restriction digestion with PflMI to detect a restriction fragment length polymorphism introduced by the mutation (18). The presence of *skn-1*(*zu135*) was verified by scoring for maternal-effect lethality.

Generation of transgenic animals. The 500-bp and 1-kb *aip-1p*:*GFP* reporters were generated via PCR using genomic DNA from the SJ4003 strain as a template (oligonucleotide sequences are available upon request). The resulting PCR products were subcloned into pPD95.75 (Addgene Inc., Cambridge, MA) digested with BamHI and XhoI as a BglII-and-XhoI fragment. The resulting plasmids were then sequenced to confirm the promoter sequence. These plasmids were prepared for bombardment by insertion of the *unc-119* marker gene into the ampicillin resistance gene on the vector backbone via homologous recombination using p*unc-119c* (16). The resulting plasmid was used to bombard DP38 [*unc-119*(*ed3*)] as previously described (5, 66). Transgenic strains were identified by rescue of the *unc-119* mutant phenotype. Strains ALF115 [*unc-119*(*ed3*) *bafIs115*] and ALF116 [*unc-119*(*ed3*) *bafIs116*] are described here.

The 1-kb *aip-1p*:*GFP* reporter lacking both *skn-1* binding sites was prepared by site-specific mutagenesis using the QuikChange Lightning multisite-directed mutagenesis kit (Stratagene Inc., La Jolla, CA). Both WWTRTCAT *skn-1* binding sites were changed to WWTCTGCAG, which has been shown to abolish *skn-1* binding and can be recognized by the restriction enzyme PstI (oligonucleotide sequences are available upon request) (2). The resulting plasmid was sequenced to verify its sequence and then used for bombardment as described above. Strains ALF117 [*unc-119*(*ed3*) *bafEx117*], ALF118 [*unc-119*(*ed3*) *bafEx118*], ALF119 [*unc-119*(*ed3*) *bafEx119*], ALF120 [*unc-119*(*ed3*) *bafEx120*], ALF121 [*unc-119*(*ed3*) *bafEx121*], ALF122 [*unc-119*(*ed3*) *bafEx122*], ALF123 [*unc-119*(*ed3*) *bafEx123*], ALF124 [*unc-119*(*ed3*) *bafEx124*], ALF125 [*unc-119*(*ed3*) *bafEx125*], and ALF126 [*unc-119*(*ed3*) *bafEx126*] were obtained and used for further analysis.

RNAi treatment. The *fah-1* RNAi vector was previously described (18). Vectors for *aip-1*, *hsf-1*, *hsp-1*, *hsp-3*, *hsp-6*, *pas-5*, *pas-6*, *pbs-*3, *pbs-6*, *pbs-7*, *rpn-1*, *rpn-8*, *rpn-11*, and *skn-1* were drawn from the Ahringer library and confirmed by sequencing (31). RNAi was delivered by feeding as previously described, with the exception that the concentration of carbenicillin was increased to 50 μg/ml and

the isopropyl β-D-thiogalactopyranoside (IPTG) concentration was decreased to 1 mM (18). RNAi mixing experiments were performed by growing separate overnight cultures of each clone and mixing equal volumes immediately before spotting onto plates. We have previously shown that diluting *fah-1*(*RNAi*) has no effect on the resulting phenotype (18).

***Q35* aggregate assay.** Eggs were extracted using hypochlorite treatment, placed on control or *fah-1*(*RNAi*) plates, and grown at 23°C for 3 days. Aggregates were scored as described previously (45). We found that placing the worm plates on ice for 5 min facilitated the scoring of worms by decreasing movement. Digital photographs were captured using an Olympus BX51 upright microscope and DP70 camera as previously described (18). All of the images and counts shown in Fig. 11 were obtained in parallel on the same day to facilitate comparison.

***aip-1*:*GFP* expression.** Eggs were isolated from SJ4003 worms or other mutants carrying the *aip-1p*:*GFP* transgene via hypochlorite treatment and placed on plates spotted with interfering RNA. Effects on *aip-1*:*GFP* expression were assessed by digital photography using the same microscope and camera as described above in day 1 adult worms (18). Treatment of adult worms with RNAi was also performed by placing day 1 adult worms on RNAi and assessing the effects 48 h later. ImageJ (NIH) was used to quantify the relative fluorescence of images, and the image data were subsequently analyzed in Prism5 (GraphPad Software, San Diego, CA) (1).

***gst-4*:*GFP* expression.** Eggs were isolated from CL2166 worms via hypochlorite treatment and placed on plates spotted with interfering RNA. Effects on *gst-4*:*GFP* expression were assessed by digital photography using the same microscope and camera used as described above for day 1 adult worms (18). All of the images in a panel were captured on the same day using identical camera settings to facilitate comparison. ImageJ (NIH) was used to quantify the relative fluorescence of images, and the image data were subsequently analyzed in Prism5 (GraphPad Software, San Diego, CA) (1).

Q-PCR quantification of GFP and *aip-1* transcript levels. Eggs were extracted from SJ4003 worms by hypochlorite treatment and grown on plates spotted with either *fah-1*(*RNAi*) or control interfering RNA for 3 days. Worms were collected by floatation, rinsed in water, and snap-frozen. Worm lysis and RNA extraction were done with the miRNeasy Mini kit (Qiagen Inc., Valencia, CA). RNA concentration was measured using a Nanodrop spectrophotometer, and 500 ng of RNA was reverse transcribed using Moloney murine leukemia virus reverse transcriptase (Promega, Madison, WI). Quantitative PCR (Q-PCR) was performed using the *Power*SYBR green PCR Master Mix (Applied Biosystems, Foster City, CA) with a Stratagene MX3000P thermocycler (Stratagene Products, La Jolla, CA). Amplification was performed using oligonucleotides designed with the PerlPrimer program for green fluorescent protein (GFP) and *aip-1* (42). These oligonucleotides cross intron-exon borders and amplify 100- to 200-bp regions (oligonucleotide sequences are available upon request). The effectiveness of the oligonucleotides was validated via obtaining a single correct-size PCR product on an agarose gel, via melting analysis on the Q-PCR machine, and via Q-PCR on serially diluted cDNA as described previously (41). Primers for *ama-1* have been previously described (55). The relative expression of GFP and *aip-1* normalized to *ama-1* expression was determined via the $2^{-\Delta\Delta Ct}$ method (41).

SA treatment. Succinylacetone (SA) was added to molten nematode growth agar (NGA) medium, and the plates were used within 1 week of pouring and spotting with OP50 because SA appears to be unstable in aqueous solution. To assess the effects of SA on *Q35*:*YFP* aggregation, AM140 or *tatn-1*(*baf1*) *rmIs132* eggs were extracted using hypochlorite treatment, arrested overnight in S-basal (0.1 M Nacl, 0.05 M K_3PO_4, pH 6.0), and placed on NGA medium plates containing 1 mg/ml SA (Sigma-Aldrich, St. Louis, MO). Yellow fluorescent protein (YFP) aggregates were counted 2 days later following incubation at 23°C. To assess the effects of SA on *aip-1p*:*GFP* expression, SJ4003 eggs were isolated using hypochlorite treatment, arrested overnight in S-basal, and placed on NGA medium plates containing 0.5 or 1.0 mg/ml SA. Effects on GFP expression were assessed by digital photography 3 days later following incubation at 20°C. Worms treated with SA fail to reach adulthood, as previously shown (18).

Xenobiotic treatment. For juglone, day 1 adult worms were treated with 38 μM juglone (Sigma-Aldrich, St. Louis, MO) in M9 (6 g Na_2HPO_4, 3 g KH_2PO_4, 5 g NaCl, 0.25 g $MgSO_4 \cdot 7H_2O$ per liter) for 1 h before being washed in M9 and being transferred to plates at 20°C (11). Juglone powder was dissolved in 100% ethanol at a 100× concentration fresh before each experiment. A control consisting of worms treated with a similar volume of 100% ethanol was performed in parallel and used for reference. Effects on GFP expression were measured 24 h later.

For tunicamycin, day 1 adult worms were treated with 5 μg/ml tunicamycin on spotted NGA medium plates for 5 h before being washed in M9 and being transferred to plates at 20°C (9). Tunicamycin was dissolved in dimethyl sulfoxide (DMSO). A control consisting of worms treated with a similar volume of DMSO was performed in parallel and used for reference. Effects on GFP expression were measured 24 h later.

For NaCl, day 1 adult worms were transferred to NGA medium plates containing 51, 200, or 400 mM NaCl and incubated at 20°C as previously described (12). Effects on GFP expression were assessed 24 h later.

Western blotting. TJ1060 eggs were put on control or *fah-1*(*RNAi*) plates, grown at 20°C for 2.5 days, and then shifted to 25°C to sterilize the animals. Alternatively, N2, ALF103, or ALF114 eggs were put on control or *fah-1*(*RNAi*) plates and grown at 20°C for 3 days. Protein was extracted from worms by boiling in LDS loading buffer (Invitrogen, Carlsbad, CA) supplemented with 10 μM *N*-ethylmaleimide. A 4.5-μg sample of protein, as determined by Bradford assay (Pierce, Rockford, IL), was subjected to 10% sodium dodecyl sulfate-polyacrylamide gel electrophoresis (SDS-PAGE) and blotted onto nitrocellulose. Blots were probed with antiubiquitin antibody (P4D1; Santa Cruz Biotechnologies, Santa Cruz, CA) at 1:100 or antiactin antibody (Cell Signaling, Danvers, MA) at 1:1,000, followed by IRDye 680 goat anti-rabbit antibody for actin and IRDye 800 donkey anti-mouse antibody for ubiquitin as recommended by the manufacturer (Li-Cor Biosciences, Lincoln, NE). Blots were imaged on a Li-Cor Odyssey system.

RESULTS

Impaired tyrosine metabolism activates AIRAP/*aip-1* expression. The amino acid tyrosine is degraded to energy via a five-step enzymatic pathway in worms and other eukaryotes (Fig. 1). We have recently identified and characterized the genes in the worm metabolic pathway (18). Treatment of worms with *fah-1*(*RNAi*), which affects the last enzyme in the pathway, produces a phenotype consisting of small body size, reduced fertility, destruction of the intestine, and reduced survival (18). This phenotype depends on the buildup of the reactive intermediates fumarylacetoacetate and maleylacetoacetate, as RNAi or genetic mutations affecting the upstream enzymes *tatn-1*, *hpd-1*, and *hgo-1* suppress the effects of *fah-1*(*RNAi*) (18). The *tatn-1*(*baf1*) mutant was isolated in a genetic screen due to resistance to the effects of *fah-1*(*RNAi*) on worm morphology, as shown by the larger body size and preserved intestinal morphology (arrows, Fig. 2E) (18). This allele has a P224S mutation which affects a highly conserved proline found in the tyrosine aminotransferase genes from worms, flies, mice, and humans (18). The *hpd-1*(*ok1955*) mutant has a 41-bp insertion followed by a 1,363-bp deletion which removes part of the first and third exons along with the entire second exon (WormBase; L. Nash, A. A. Ferguson, and A. L. Fisher, unpublished data). This mutant is also resistant to the effects *fah-1*(*RNAi*) (Fig. 2E).

We have shown that tyrosine metabolites produce both oxidative and ER stress in worms (18). The AIRAP/*aip-1* proteins are induced by environmental stressors, such as arsenic, that produce both oxidative and ER stress (56, 57). Hence, we hypothesized that the tyrosine metabolites may activate *aip-1* expression. We examined whether *aip-1* is activated following exposure to tyrosine metabolites produced by *fah-1*(*RNAi*) and found that *fah-1*(*RNAi*) was a robust activator of an *aip-1p*:*GFP* reporter gene in transgenic worms (Fig. 2A and B). To confirm that the increase in GFP expression reflected an increase in the expression of the endogenous *aip-1* gene, we used Q-PCR to quantify both the GFP transcript and the *aip-1* transcript in control or *fah-1*(*RNAi*)-treated animals (Fig. 2C). We found that *fah-1*(*RNAi*) significantly increased the expression of both, with *aip-1* showing 3.8-fold induction and GFP showing 11.1-fold induction. Hence, changes in reporter ex-

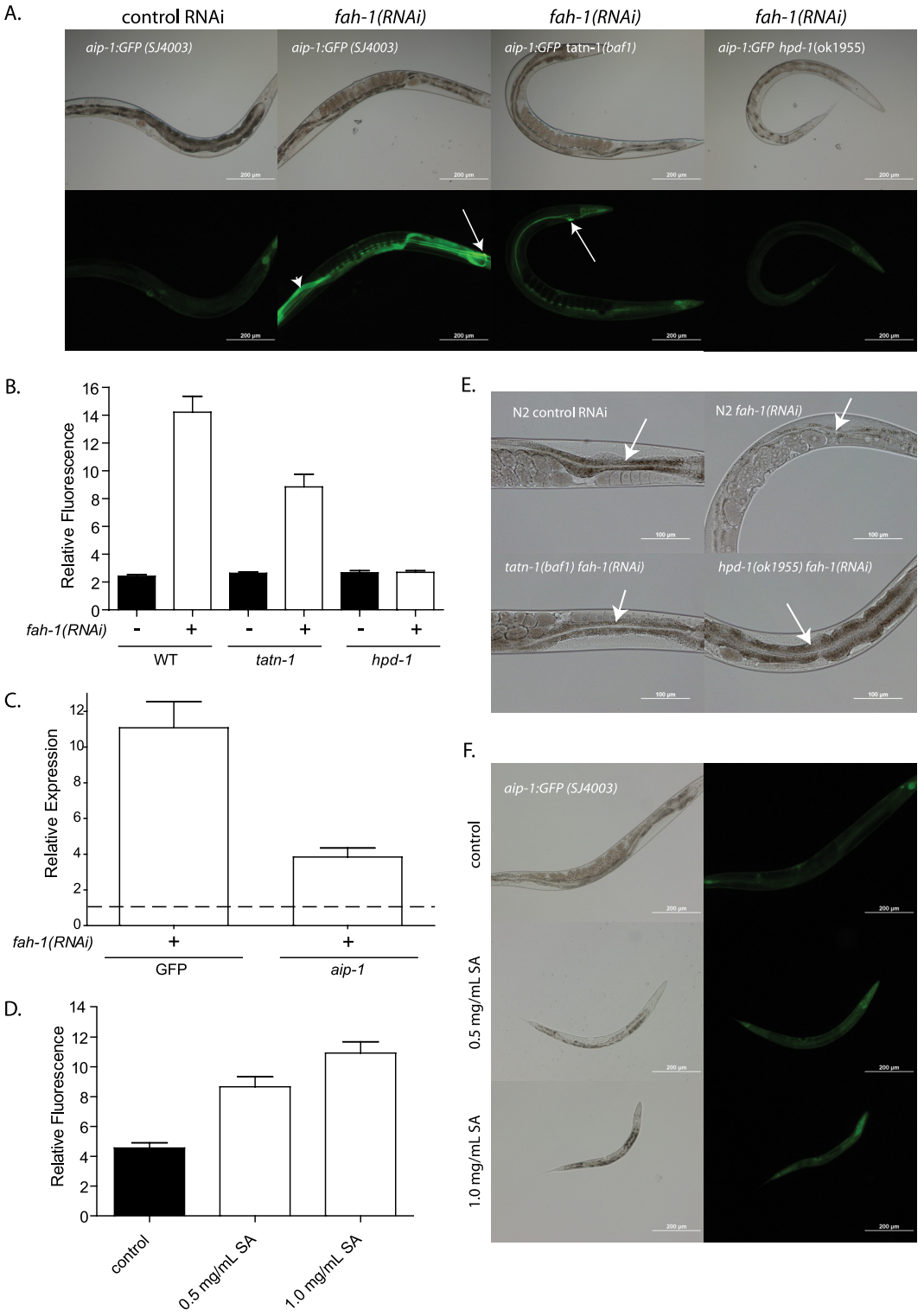

FIG. 2. Tyrosine metabolites induce *aip-1* expression. (A) Digital images showing the effects of control or *fah-1*(*RNAi*) treatment on SJ4003 (*aip-1p*:*GFP*) worms or *tatn-1*(*baf1*) and *hpd-1*(*ok1955*) mutants carrying the *aip-1p*:*GFP* transgene. Worms were treated with *fah-1*(*RNAi*) from egg hatching, and day 1 adult worms were photographed to examine GFP expression. The intestine (arrowhead) and excretory cell (arrow) are indicated. (B) Graph of fluorescence measured from digital images [$n = 15$ for all; $P < 0.0001$ for the wild-type (WT) control versus *fah-1*(*RNAi*), $P < 0.0001$ for the *tatn-1*(*baf1*) control versus *fah-1*(*RNAi*), $P = 0.44$ for the *hpd-1*(*ok1955*) control versus *fah-1*(*RNAi*), $P = 0.0006$ for WT *fah-1*(*RNAi*) versus *tatn-1*(*baf1*) *fah-1*(*RNAi*), and $P < 0.0001$ for *hpd-1*(*ok1955*) *fah-1*(*RNAi*)]. (C) Graph showing relative expression of GFP and the endogenous *aip-1* gene in SJ4003 worms treated with *fah-1*(*RNAi*) [$n = 5$ biological replicates; $P = 0.0024$ for the *aip-1* control versus *fah-1*(*RNAi*) and $P = 0.0004$ for GFP]. (D) Graph of fluorescence measured from digital images in panel F showing the effects of treatment of SJ4003 with SA from egg hatching (control versus SA, $P < 0.0001$ for both by *t* test; $n = 15$ for all). (E) Digital images showing morphological effects of control or *fah-1*(*RNAi*) treatment of N2, *tatn-1*(*baf1*), and *hpd-1*(*ok1955*). (Arrow = intestine) (F) Images showing the effect of 0.5 or 1.0 mg/ml SA on 3-day-old worms. SA treatment impairs the development of worms into reproductive adults.

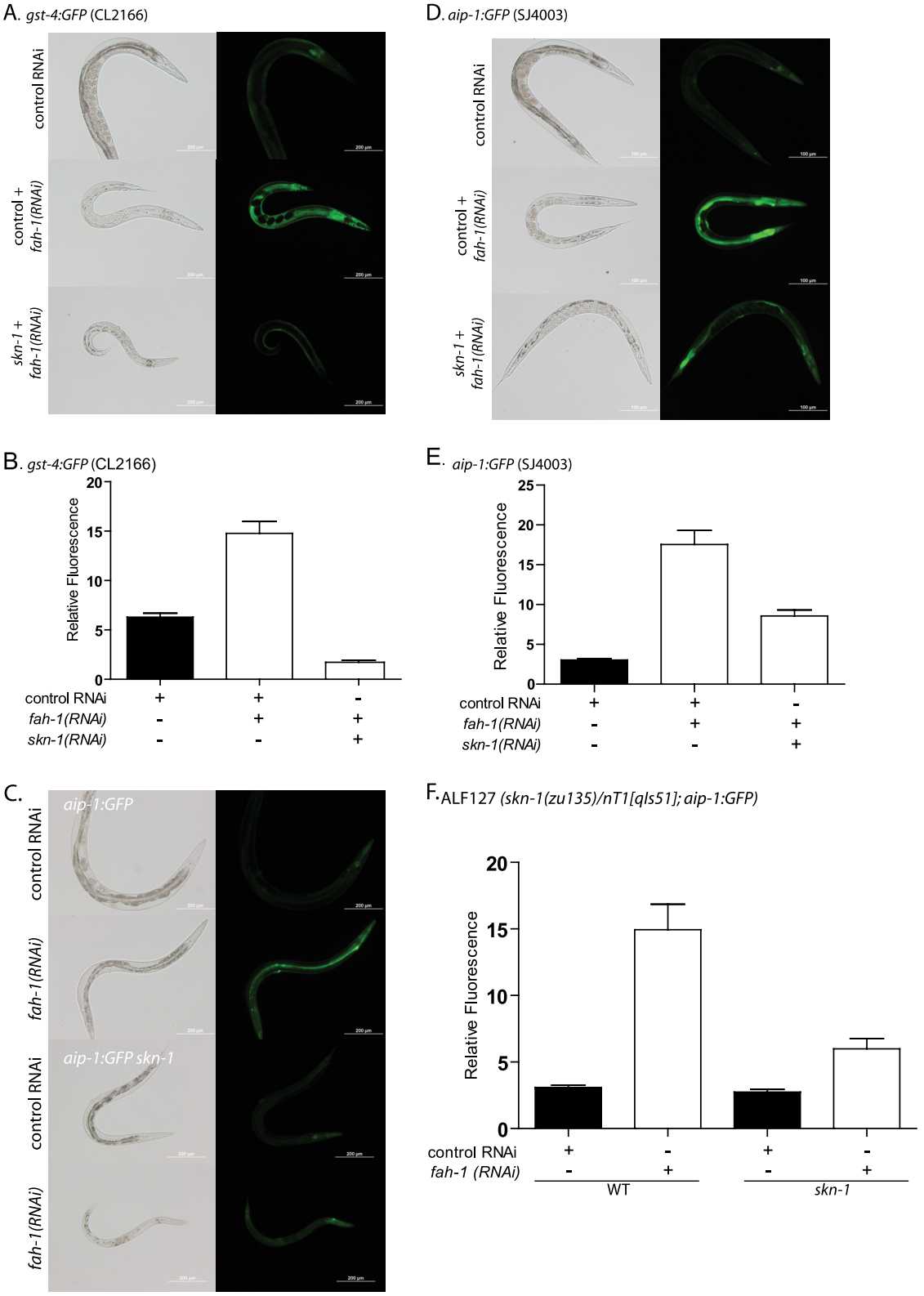

FIG. 3. *skn-1* is activated by tyrosine metabolites and is necessary for full activation of *aip-1* expression. (A) Digital images showing the effects of treatment of CL2166 (*gst-4p*:*GFP*) worms with control interfering RNA, a 1:1 mixture of *fah-1* and control interfering RNA, or a 1:1 mixture of *fah-1* and *skn-1*(*RNAi*). (B) Graph of fluorescence measured from digital images [$n > 20$ for all; $P < 0.0001$ for *fah-1* and control interfering RNA versus *fah-1* and *skn-1*(*RNAi*)]. (C) Digital images showing the effects of treating SJ4003 or ALF127 {*skn-1*(*zu135*)/*nT1*[*qIs51*] *aip-1p*:*GFP*} transgenic worms with *fah-1* or control interfering RNA. (D) Images showing the effects of treatment of SJ4003 worms with control interfering RNA, a 1:1 mixture of *fah-1* and control interfering RNA, or a 1:1 mixture of *fah-1* and *skn-1*(*RNAi*). (E) Graph of fluorescence measured from digital images in panel D [$n = 15$ for all; $P < 0.0001$ for control interfering RNA versus *fah-1* and control interfering RNA or *fah-1* and *skn-1*(*RNAi*)]. (F) Graph of fluorescence measured from the digital images in panel C [$n = 15$ for all; $P < 0.0001$ for the wild-type (WT) control versus *fah-1*(*RNAi*) and $P = 0.0003$ for the *skn-1* control versus *fah-1*(*RNAi*)].

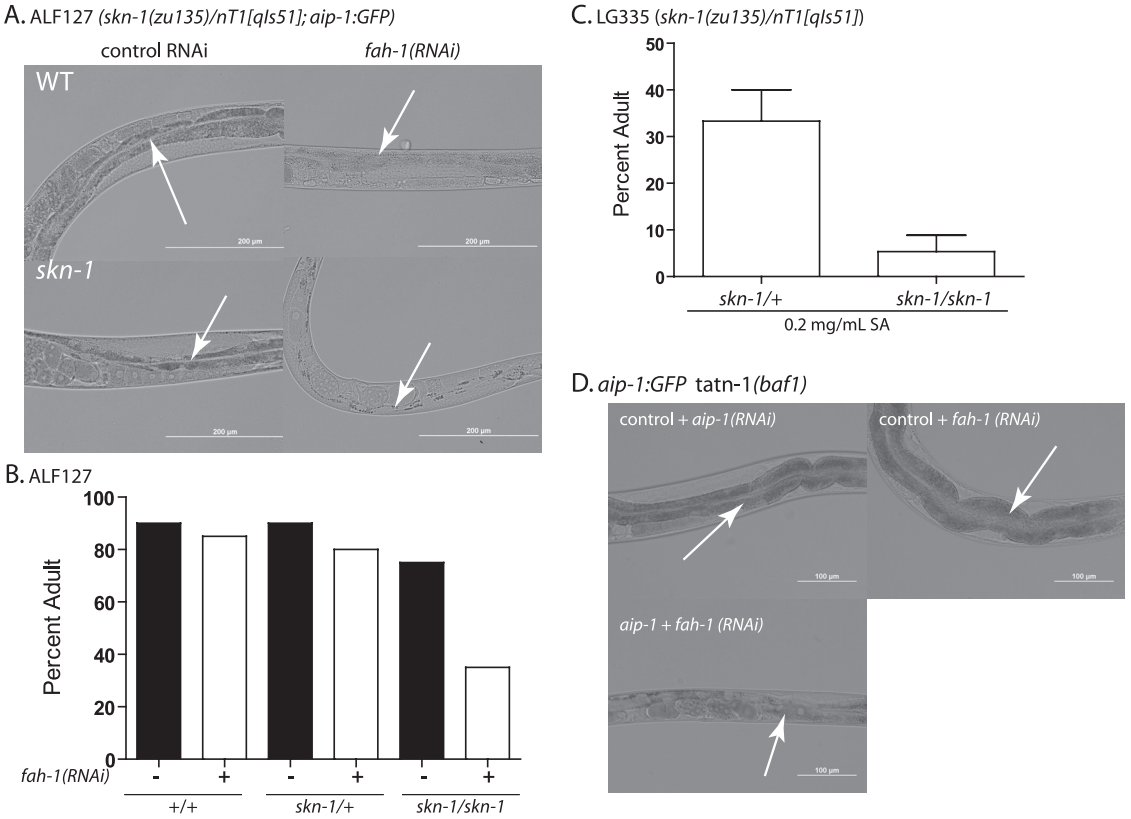

FIG. 4. *skn-1* protects worms against tyrosine metabolites. (A) Digital images of wild-type (WT) and *skn-1* mutant worms treated with *fah-1*(*RNAi*) showing increased damage to the intestine in *skn-1 fah-1*(*RNAi*)-treated worms (arrow = intestine). (B) Graph showing the percentages of adult animals among wild-type, *skn-1* heterozygous, and *skn-1* homozygous worms treated with control or *fah-1*(*RNAi*) ($n = 20$ for all). (C) Graph showing the percentages of adult animals among *skn-1* heterozygous and *skn-1* homozygous worms treated with 0.2 mg/ml SA (three replicates of 25 worms each; $P = 0.01$ by t test). (D) Digital images showing the effects of treatment of ALF103 [*tatn-1*(*baf1*)] worms with a 1:1 mixture of *fah-1* and control interfering RNA, *aip-1* and control interfering RNA, or *fah-1* and *aip-1*(*RNAi*). The image for *fah-1* and *aip-1*(*RNAi*) represents ~10% of the animals and <1% in the other treatments.

pression reflect changes in the expression of the endogenous *aip-1* gene. Notably, in treated worms, the expression of GFP is seen both in the intestine (Fig. 2A, arrowhead), which expresses *fah-1* and presumably has direct exposure to these reactive metabolites, and also in the excretory cell, which does not express *fah-1* (Fig. 2A, arrow) (18).

To verify that tyrosine metabolites were directly responsible for the induction of *aip-1p*:*GFP*, we created transgenic worms carrying the transgene and the *tatn-1*(*baf1*) and *hpd-1*(*ok1955*) mutations (Fig. 1). When the worms were treated with *fah-1*(*RNAi*), both mutations suppressed the morphological effects of RNAi treatment due to the decreased accumulation of fumarylacetoacetate and maleylacetoacetate (Fig. 1 and 2E). Consistent with the reduced accumulation of metabolites, both the *hpd-1*(*ok1955*) and *tatn-1*(*baf1*) mutants showed reduced GFP expression following RNAi treatment (Fig. 2A and B). This finding is consistent with a direct effect of tyrosine metabolites on the expression of *aip-1*.

Notably, the *hpd-1*(*ok1955*) mutation completely suppressed the increase in GFP expression following *fah-1*(*RNAi*) treatment, while the *tatn-1*(*baf1*) mutant showed an intermediate phenotype with retained induction in the excretory cell (Fig. 2A and B). This may reflect the differing strengths of the *hpd-1*(*ok1955*) mutation, which is a 1,363-nucleotide deletion, versus *tatn-1*(*baf1*), which is a point mutation, in terms of the flux through the tyrosine degradation pathway (18). We suspect that *tatn-1*(*baf1*) is a hypomorphic allele, as the *tatn-1*(*ok3323*) allele, which is a 602-nucleotide deletion in exon 2, is lethal (WormBase; A. L. Fisher, unpublished data). However, the similarity between *hpd-1*(*ok1955*) and *tatn-1*(*baf1*) with regard to resistance to the adverse effects of *fah-1*(*RNAi*) on morphology (Fig. 2E) or *Q35*:*YFP* aggregation (see below) is consistent with a protective effect of *aip-1* induction in the *tatn-1*(*baf1*) mutants.

We also treated wild-type worms carrying the *aip-1p*:*GFP* transgene with SA. SA is produced *in vivo* from the tyrosine metabolites maleylacetoacetate and fumarylacetoacetate via nonenzymatic isomerization and decarboxylation, and SA is the only commercially available metabolite (39, 43). We have previously shown that treatment of worms with SA mimics the phenotype produced by *fah-1*(*RNAi*) (18). We found that the treatment of worms with 0.5 or 1.0 mg/ml SA induced the expression of *aip-1* (Fig. 2D and F). These findings demonstrate that tyrosine degradation products are the first identified endogenous activator of the *aip-1*/AIRAP pathway.

The *skn-1* transcription factor regulates *aip-1* expression. The oxidative-stress-sensitive transcription factor *skn-1* has been

previously shown to be involved in the transcriptional activation of *aip-1* in arsenic-treated worms (57). Similarly to arsenic, we have previously shown that tyrosine metabolites produce oxidative stress in *fah-1*(*RNAi*)-treated worms (18). Consequently, we tested whether the previously demonstrated activation of the oxidative-stress-responsive *gst-4* gene by *fah-1*(*RNAi*) depends on *skn-1* and whether the activation of *aip-1* also requires *skn-1*.

The *gst-4* gene was identified as an oxidative-stress-responsive gene, and a *gst-4p*:*GFP* reporter gene shows *skn-1*-dependent activation to multiple sources of oxidative stress (11, 30, 40, 60). Treatment of *gst-4p*:*GFP* transgenic worms with a 1:1 mixture of control interfering RNA and *fah-1*(*RNAi*) produced a robust activation of the reporter, which is consistent with our prior finding that a similar dilution of *fah-1*(*RNAi*) does not reduce the phenotype produced (Fig. 3A and B) (18). In contrast, treatment with a mixture of *skn-1*(*RNAi*) and *fah-1*(*RNAi*) resulted in no induction of the reporter (Fig. 3A and B). This finding is consistent with the activation of *skn-1* following the accumulation of tyrosine metabolites and a subsequent absolute requirement for *skn-1* to induce *gst-4* expression.

However, similar RNAi treatment of *aip-1p*:*GFP* transgenic worms produced distinct results, as treatment of worms with a 1:1 mixture of *fah-1*(*RNAi*) and control interfering RNA produced a strong induction of GFP expression (Fig. 3D and E). But treatment with a mixture of *skn-1*(*RNAi*) and *fah-1*(*RNAi*) still resulted in an increase in GFP expression (Fig. 3D and E). This increase was roughly half of the response to the *fah-1*(*RNAi*) and control interfering RNA mixture but much greater than the increase observed in treated *gst-4p*:*GFP* worms (Fig. 3A and B). The response of *aip-1* to treatment with arsenite has also been recently shown to be at least partially *skn-1* dependent (57).

To ensure that our findings were not due to an incomplete response to *skn-1*(*RNAi*), we constructed the ALF127 {*skn-1*(*zu135*)/*nT1*[*qIs51*] *aip-1p*:*GFP*} strain to genetically remove *skn-1*. The ALF127 progeny lacking *skn-1* are identified by the lack of the *myo-2*:*GFP* reporter carried on the *nT1* balancer chromosome. Consistent with our findings obtained using *skn-1*(*RNAi*), treatment of this strain with *fah-1*(*RNAi*) still produced an increase in GFP expression in the *skn-1* progeny (Fig. 3C and F). As before, this induction is significantly lower than that observed in the nonmutant SJ4003 (*aip-1p*:*GFP*) strain treated in parallel (Fig. 3C and F). We also observed increased *aip-1* expression in the *skn-1*(+) progeny of treated ALF127 worms (not shown). These findings suggest that *aip-1* expression may be under *skn-1*-dependent but also *skn-1*-independent control.

We also found that the *skn-1*(−) progeny from ALF127 appeared to be more strongly affected by *fah-1*(*RNAi*) than either wild-type worms or the *skn-1*(+) progeny from ALF127. To explore this observation, we examined ×20 images of treated worms and found that the *skn-1*(−) worms exhibited more damage to the intestine than wild-type *fah-1*(*RNAi*)-treated worms (Fig. 4A). Associated with the increase in tissue damage, we also observed an increase in larval arrest in the *fah-1*(*RNAi*)-treated *skn-1*(−) worms (Fig. 4B). Larval arrest is an uncommon phenotype in wild-type *fah-1*(*RNAi*)-treated worms, with 85% of worms reaching adulthood after 3 days while

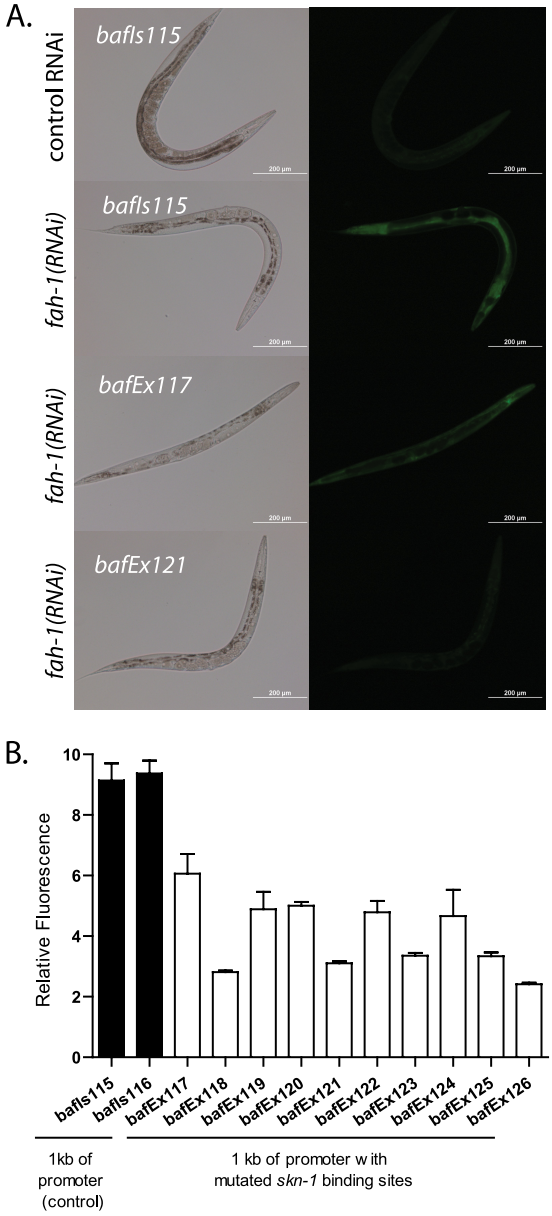

FIG. 5. *aip-1* is regulated by two *skn-1* binding sites in the promoter. (A) Digital images of transgenic worms with 1 kb of the *aip-1* promoter sequence (*bafIs115*) treated with a control or *fah-1*(*RNAi*) and images of transgenic worms with the 1-kb *aip-1* promoter transgene in which both *skn-1* binding sites have been mutated (*bafEx117* and *bafEx121*) treated with *fah-1*(*RNAi*). (B) Graph of fluorescence measured from digital images from two nonmutated control lines and nine individual transgenic worm lines carrying the mutated promoter ($n = 15$ for all; $P < 0.0001$ for mutants versus *bafIs115*, except $P = 0.0007$ for *bafEx117* and $P = 0.0001$ for *bafEx124*; $P < 0.0001$ for mutants versus *bafIs116*, except $P = 0.0001$ for *bafEx117*).

only 35% of *skn-1*(−) *fah-1*(*RNAi*)-treated worms reached adulthood. This suggested that *skn-1* mutant worms were more sensitive to the effects of tyrosine metabolites. To test this hypothesis, we treated *skn-1* mutants, LG335 {*skn-1*(*zu135*)/*nT1*[*qIs51*]}, with 0.2 mg/ml SA, as we have previously shown that low doses of SA produce a mixture of adult worms and arrested larvae (18). We found that 33% of the *skn-1*(+) prog-

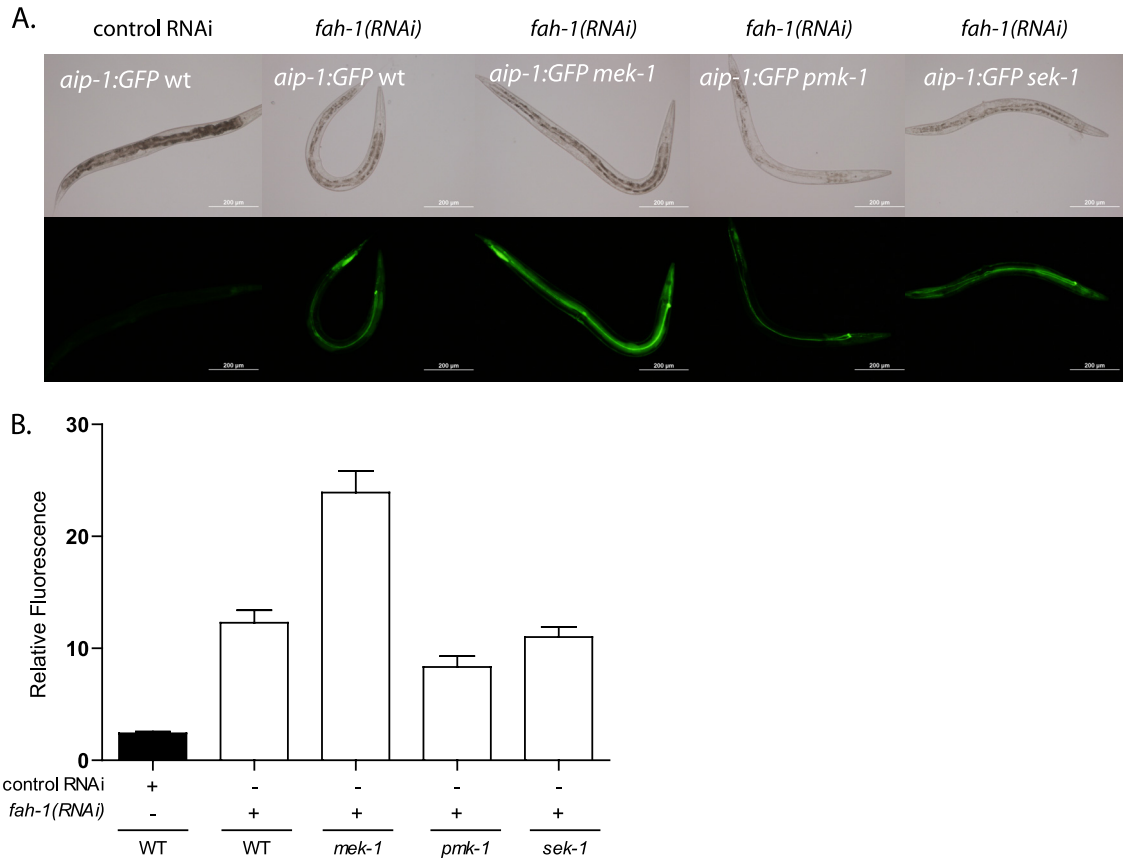

FIG. 6. Stress-responsive kinases play a minor role in the activation of *aip-1* expression. (A) Digital images of wild-type (WT) *aip-1*:*GFP* worms or *aip-1*:*GFP* worms with mutations in the *mek-1*-, *sek-1*-, or *pmk-1*-encoded kinase treated with *fah-1*(*RNAi*). (B) Graph of fluorescence measured from digital images [$n > 15$ for all; $P > 0.0001$ for wild-type *fah-1*(*RNAi*) versus *mek-1 fah-1*(*RNAi*), $P = 0.1888$ for wild-type *fah-1*(*RNAi*) versus *sek-1 fah-1*(*RNAi*), and $P = 0.0063$ for wild-type *fah-1*(*RNAi*) versus *pmk-1 fah-1*(*RNAi*)].

eny reached adulthood while only 5% of the *skn-1*(−) progeny reached adulthood (Fig. 4C). To test whether this protective effect of *skn-1* involved *aip-1*, we treated the *tatn-1*(*baf1*) mutant with either a 1:1 mixture of *fah-1* and control interfering RNA, *aip-1* and control interfering RNA, or *fah-1* and *aip-1*(*RNAi*) to see whether we could block the protective effect of *aip-1* suggested by the induction observed above. We found that ~10% of the *fah-1*- and *aip-1*(*RNAi*)-treated worms lost the protective effect of the *tatn-1*(*baf1*) mutation and resembled wild-type worms treated with *fah-1*(*RNAi*) (Fig. 4D). Our findings suggest that *skn-1* regulates *aip-1* as part of a protective response to reactive tyrosine metabolites. However, *aip-1* could be either a direct or an indirect target gene of *skn-1*.

aip-1 is a potential *skn-1* target gene, as the *aip-1* promoter has two WWTRTCAT consensus binding sites for *skn-1* (ATTGTCAT at −70 and AATGTCAT at −250 relative to the TATA box) within 500 bp of the transcriptional start site (2, 53). To test whether these sites are functional, we generated a series of *aip-1* promoter deletions. We found that 500 nucleotides of promoter sequence was insufficient to respond to *fah-1*(*RNAi*), but a 1-kb promoter drove GFP expression in the intestine and to a lesser extent in the excretory cell after exposure to *fah-1*(*RNAi*) (Fig. 5A and data not shown). We tested four transgenic lines which demonstrated very similar results (Fig. 5A and B and not shown). Mutation of both *skn-1* binding sites, by changing them to WWTCTGCAG, which prevents *skn-1* binding in other target genes, in the 1-kb promoter resulted in a reduction in GFP expression following exposure to *fah-1*(*RNAi*) (Fig. 5A and B) (2). Mutation of the binding sites also had no detectable effect on the basal GFP expression which was low in both the mutants and the control (data not shown). Of nine transgenic lines tested, none was comparable to the lines generated with the nonmutated promoter (Fig. 5A and B). However, several of the transgenic lines harboring the reporters with mutated binding sites still demonstrated variable GFP induction following RNAi treatment (Fig. 5B). This observation is consistent with *aip-1* being a direct target of *skn-1* and also being the target of a *skn-1*-independent pathway(s).

In worms, the *skn-1*-dependent responses to oxidative stress involve the actions of several kinases which directly or indirectly regulate the nuclear localization and transcriptional activity of *skn-1* (3, 26, 33). Further, tyrosine metabolites have been shown to activate ERK kinases in mammalian cells (28). Given these observations and the involvement of *skn-1* in *aip-1* regulation, we asked whether the upstream stress-responsive kinase-encoding gene *mek-1*, *sek-1*, or *pmk-1* is required for the expression of *aip-1*. We crossed the *aip-1p*:*GFP* reporter into worms lacking each of these kinase genes and then used *fah-1*(*RNAi*) to investigate the responses to this stressor. We found

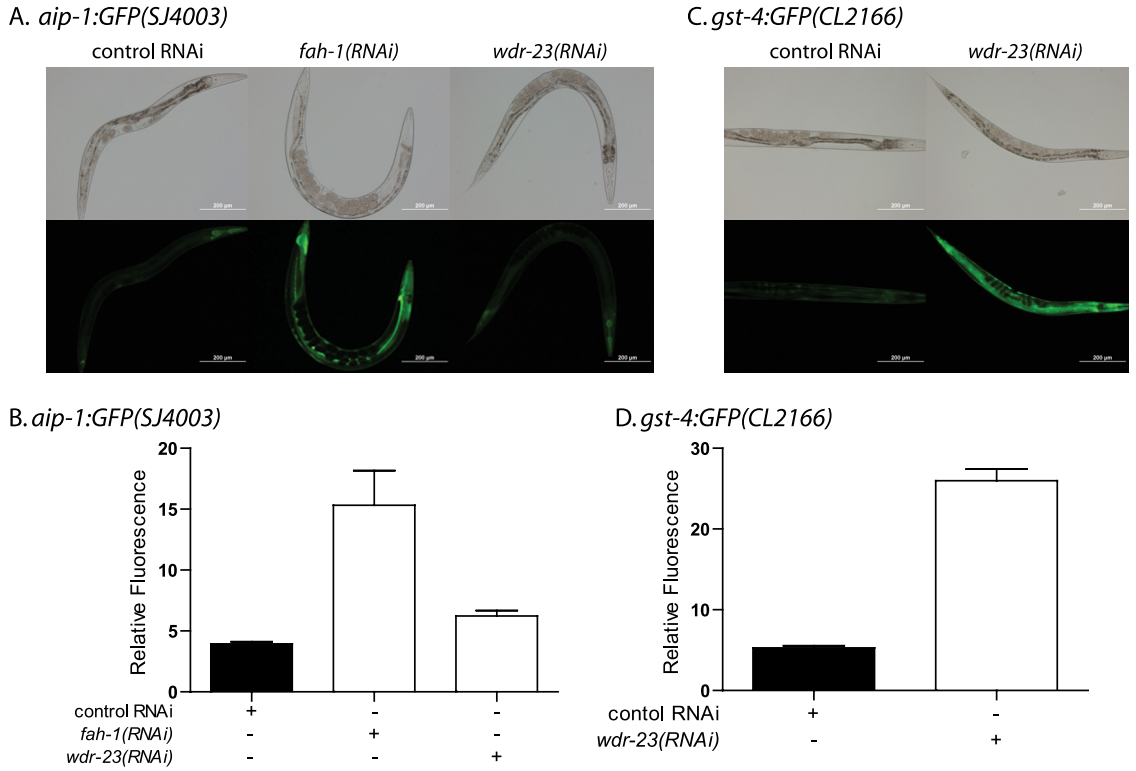

FIG. 7. *skn-1* is not sufficient for *aip-1* expression. (A) Digital images showing the effects of control, *fah-1*, and *wdr-23*(*RNAi*) treatments of SJ4003 (*aip-1p*:*GFP*) transgenic worms. (B) Graph of fluorescence measured from digital images ($n > 15$ for all; $P < 0.0001$ for *wdr-23* versus control interfering RNA, $P = 0.0007$ for *fah-1* versus control interfering RNA). (C) Images showing the effects of control and *wdr-23*(*RNAi*) treatments on CL2166 (*gst-4p*:*GFP*) transgenic worms. (D) Graph of fluorescence measured from digital images ($n = 10$ for all; $P < 0.0001$ for *wdr-23* versus control interfering RNA).

that loss of *sek-1* marginally reduced the expression of *aip-1p*:*GFP*, whereas loss of *pmk-1* showed a statistically significant but still rather modest reduction in the induction of *aip-1* following treatment (Fig. 6). This is consistent with either a mode of *skn-1* activation independent of these kinases or compensation by other activators of *aip-1* expression.

To further explore the role of *skn-1* in the regulation of *aip-1*, we directly activated *skn-1* via the treatment of worms with *wdr-23*(*RNAi*). The *wdr-23* gene encodes a WD-40 repeat protein which has been recently shown to bind *skn-1* and regulate its degradation (11). Both mutation of *wdr-23* and *wdr-23*(*RNAi*) have been shown to lead to *skn-1* nuclear localization and produce strong induction of *skn-1* target genes (11). Consistent with these observations, we found that treatment of *gst-4p*:*GFP* transgenic worms with *wdr-23*(*RNAi*) led to a dramatic increase in GFP expression relative to control interfering RNA (Fig. 7C and D). However, treatment of *aip-1p*:*GFP* transgenic worms produced a minimal increase in GFP expression (Fig. 7A and B). Our results suggest that while *aip-1* is a direct target gene of *skn-1*, *aip-1* is likely not solely regulated by *skn-1*, and *skn-1* likely requires other transcription factors to induce *aip-1* expression.

***aip-1* is also regulated by *hsf-1* in response to tyrosine metabolites.** In worms, *aip-1* has been shown to be upregulated in response to heat shock, and the induction of *aip-1* is dependent on *hsf-1*, which is the worm homolog of heat shock factor (25). To test whether *hsf-1* could be an additional regulator of *aip-1* expression in response to *fah-1*(*RNAi*), we treated worms with control interfering RNA, control interfering RNA mixed 1:1 with *fah-1*(*RNAi*), 1:1 *fah-1*(*RNAi*) and *hsf-1*(*RNAi*), or 1:1 *hsf-1*(*RNAi*) and control interfering RNA. We found that treatment with *fah-1* and *hsf-1*(*RNAi*) together reduced the activation of *aip-1* relative to *fah-1* and control interfering RNA (Fig. 8A and B). This finding suggests that the full expression of *aip-1* depends on both *hsf-1* and *skn-1*.

Misfolded proteins and proteosome dysfunction contribute to *aip-1* expression. Our results suggested that oxidative stress contributes to *aip-1* regulation but that an additional effect of tyrosine metabolites is important in triggering expression. To explore the types of cell damage that induce *aip-1* expression, we tried several pharmacologic and RNAi treatments.

Recent microarray data suggested that the xenobiotic juglone activates the expression of *aip-1*, so we tested the effect of this compound on *aip-1p*:*GFP* transgenic worms (53). We found that treatment of worms with 38 μM juglone significantly increased GFP expression 24 h following treatment (Fig. 9A and D). Juglone is similar to tyrosine metabolites because juglone produces oxidative stress, ER stress, and direct covalent damage to proteins (61). To explore whether ER stress is sufficient to induce *aip-1* expression, we treated *aip-1p*:*GFP* transgenic worms with tunicamycin. Treatment of worms with 5 μg/ml tunicamycin produces a minimal increase in GFP expression relative to the control, which is consistent with prior results obtained with cultured cells (56). This dose of tunica-

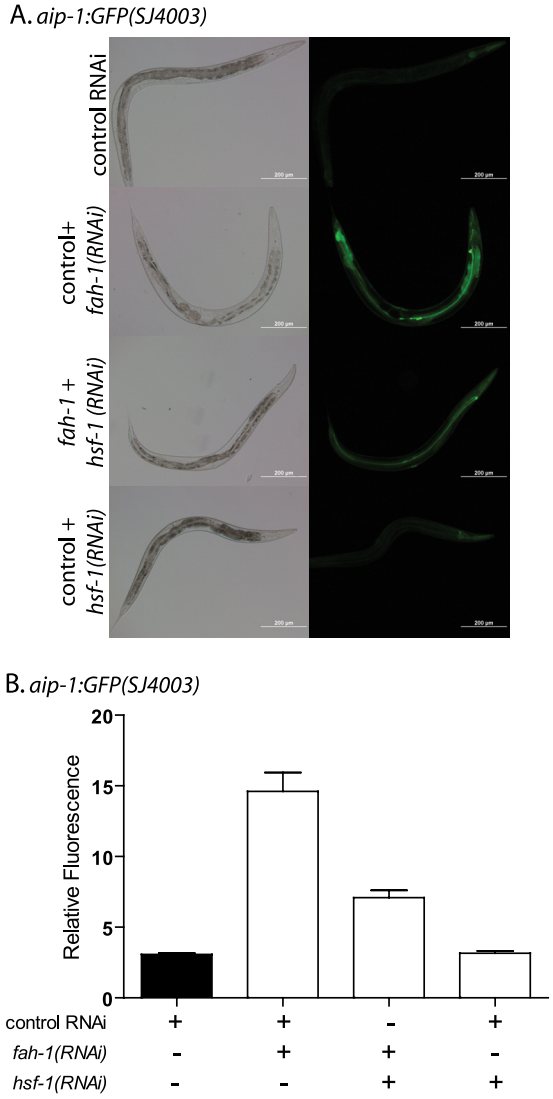

FIG. 8. *hsf-1* is required for *aip-1* expression produced by tyrosine metabolites. (A) Digital images of SJ4003 (*aip-1p*:*GFP*) worms treated with the control, a 1:1 mixture of the control and *fah-1*(*RNAi*), a 1:1 mixture of *fah-1* and *hsf-1*(*RNAi*), and a 1:1 mixture of the control and *hsf-1*(*RNAi*). (B) Graph of fluorescence measured from digital images [$n > 15$ for all; $P < 0.0001$ for the control versus the control and *fah-1*(*RNAi*) and $P < 0.0001$ for the control and *fah-1*(*RNAi*) versus *hsf-1* and *fah-1*(*RNAi*)].

mycin robustly activates the ER stress response, as indicated by the *hsp-4p*:*GFP* reporter gene (data not shown). Finally, we placed worms under hypertonic conditions via exposure to 200 or 400 mM NaCl. Hypertonic stress has been shown to enhance protein aggregation and lead to an increase in cellular glycerol content (12, 37, 38). This stress fails to induce GFP expression above the control level (Fig. 9B and D). Together, our results suggested that xenobiotics that produce multiple types of cell stress serve to induce *aip-1* expression, while ER stress or protein aggregation alone may not be sufficient.

We hypothesized that the accumulation of damaged and misfolded proteins could serve as a trigger for *aip-1* expression, as the oxidative stress and direct protein damage produced by juglone, arsenic, or tyrosine metabolites could then synergize with the accumulation of ER proteins targeted for ER-associated degradation. To test this hypothesis, we treated worms with RNAi against *hsp-1*, *hsp-3*, and *hsp-6*, which are involved in the maintenance of proteostasis in the cytoplasm, ER, or mitochondria, respectively (32, 46, 62). We found that *hsp-1*(*RNAi*) and *hsp-3*(*RNAi*) both induce *aip-1p*:*GFP*, while *hsp-6*(*RNAi*) produced a lesser induction (Fig. 9A and D). As *hsp-1*(*RNAi*) produced larval arrest when started at egg hatching, we also repeated the experiments with *hsp-1* and *hsp-3*(*RNAi*) in adult worms to exclude a developmental effect on *aip-1* expression. We found that both RNAi treatments induced GFP expression in adults after 48 h of treatment (Fig. 9C and E), which shows that *aip-1* expression is independent of development.

Worms treated with *hsp-1* or *hsp-3*(*RNAi*) would be expected to accumulate ubiquitinated proteins targeted for degradation via the proteosome. Hence, we hypothesized that inhibiting proteosomal function might mimic the effects of *hsp-1* or *hsp-3*(*RNAi*) or tyrosine metabolites and lead to *aip-1* expression. To test this hypothesis, we treated worms with RNAi against *rpn-11* (19S regulatory particle subunit) or *pbs-3* (20S β subunit) and assessed the effect on *aip-1* expression. We found that this led to strong induction of the *aip-1p*:*GFP* reporter gene in treated worms (Fig. 10A and B). Our result suggested that proteosomal dysfunction could serve to trigger *aip-1* expression. To further test this hypothesis, we chose additional proteosomal genes and inhibited them via RNAi. We found that all of the genes showed an increase in GFP expression relative to the control (Fig. 10A and B). Recently, these same clones were shown to have differing effects on *skn-1* nuclear localization and *gst-4* activation, but we found little connection between these reported effects and the effects on *aip-1* expression (30). This could be due to the involvement of *hsf-1* in *aip-1* regulation. To exclude developmental effects of proteosomal subunit RNAi on *aip-1* expression, we repeated the experiment with day 1 adults and found that RNAi treatment still increased GFP expression (Fig. 10C and D).

Impaired tyrosine degradation produces proteosomal dysfunction. We then asked whether worms treated with *fah-1*(*RNAi*) show evidence of proteosomal dysfunction. We hypothesized that these metabolites could lead to an increase in misfolded proteins and lead to relative proteosomal dysfunction. We tested this possibility in two ways.

First, *fah-1*(*RNAi*) has been shown to increase the aggregation of a synthetic polyglutamine repeat protein in *C. elegans* (49). This suggests that either *fah-1* has a novel role in protein folding or the accumulation of tyrosine metabolites by *fah-1*(*RNAi*) leads to the accumulation of aggregates. We tested these possibilities by using mutations in *tatn-1*(*baf1*) and *hpd-1*(*ok1955*), which block enzymes upstream of *fah-1* in the tyrosine degradation pathway and prevent the development of metabolic disease (18). Following treatment with *fah-1*(*RNAi*), wild-type worms expressing the *Q35*:*YFP* transgene in muscle show a marked increase in the number of YFP aggregates compared to control interfering-RNA-treated worms (Fig. 11A and B). However, worms with mutations in either *tatn-1*(*baf1*) or *hpd-1*(*ok1955*) are protected from the increase in polyglutamine aggregates following RNAi treatment (Fig. 11A and B). This suggests that the accumulation of tyrosine metab-

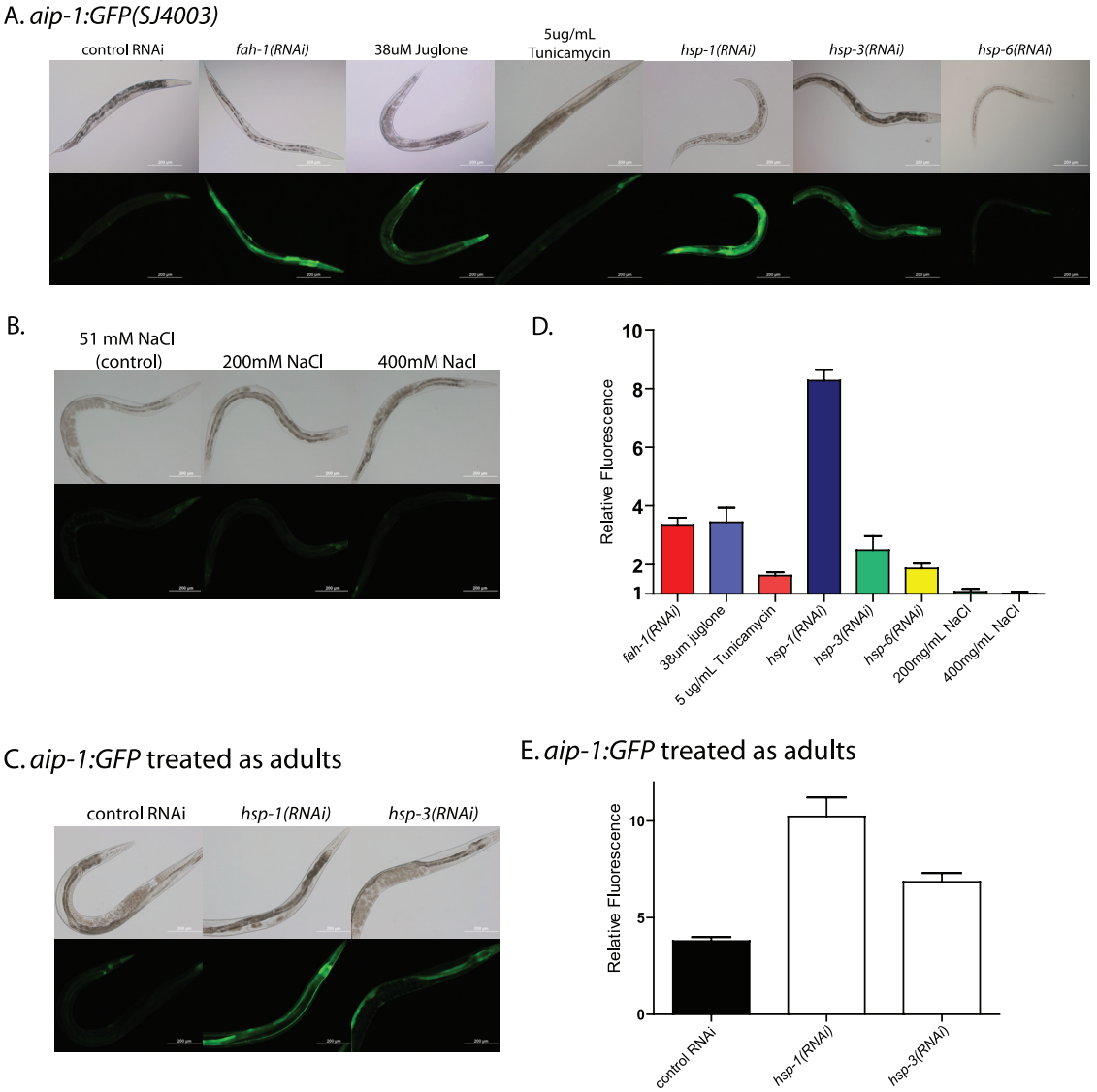

FIG. 9. Multiple proteotoxic stimuli activate *aip-1* expression. (A) Digital photos showing the effects of treatment of *aip-1p*:*GFP* transgenic worms with the xenobiotics juglone and tunicamycin or the control, *fah-1*, *hsp-1*, *hsp-3*, or *hsp-6* RNAi. (B) Digital photos showing the effect of transferring day 1 adult *aip-1p*:*GFP* transgenic worms to NGA medium plates containing 51, 200, or 400 mM NaCl for 24 h. (C) Digital images of adult worms treated with the control, *hsp-1*, or *hsp-3*(*RNAi*) for 48 h. (D) Graph of fluorescence measured from the digital images in panels A and B ($n > 10$ for all). To facilitate comparison across separate trials, the values were normalized with the mean value of the untreated control images in each trial, and this normalized value is plotted [in the individual trials, $P = 0.0002$ for juglone versus the control, $P = 0.444$ for 400 mM NaCl versus 51 mM NaCl, $P = 0.255$ for 200 mM NaCl versus 51 mM NaCl, $P = 0.001$ for tunicamycin versus the control, $P < 0.0001$ for *hsp-1* and *hsp-3*(*RNAi*) versus control interfering RNA, and $P = 0.0002$ for *hsp-6*(*RNAi*) versus control interfering RNA]. (E) Graph of fluorescence measured from the digital images in panel C [$n = 15$ for all; $P < 0.0001$ for *hsp-1* and *hsp-3*(*RNAi*) versus the control].

olites is responsible for the observed increase in protein aggregation, perhaps due to impaired proteosomal function.

To directly test if tyrosine metabolites produce aggregation of *Q35*:*YFP*, we treated worms expressing *Q35*:*YFP* with SA. We found that SA treatment of wild-type *Q35*:*YFP* transgenic worms and *tatn-1*(*baf1*) *Q35*:*YFP* transgenic worms led to an increase in aggregates in both (Fig. 11C). This demonstrates that tyrosine metabolites directly lead to an increase in polyglutamine protein aggregation and that mutations in upstream enzymes like *tatn-1* cannot block this effect.

Second, we examined whether worms treated with *fah-1*(*RNAi*) show an increase in polyubiquitinated proteins awaiting degradation by the proteosome (54). Adult worms treated with *fah-1*(*RNAi*) from egg hatching show a dramatic increase in polyubiquitinated proteins compared to control interfering-RNA-treated animals, as shown by Western blotting (Fig. 11D). This increase depends on an intact tyrosine degradation pathway, as the *tatn-1* and *hpd-1* mutations block this accumulation (Fig. 11E). The aggregation of *Q35*:*YFP* and the increase in polyubiquitinated proteins observed in *fah-1*(*RNAi*)-treated worms are consistent with relative proteosome dysfunction.

While *fah-1*(*RNAi*) produces proteosomal dysfunction, the regulation of *aip-1* by *fah-1*(*RNAi*) and *hsp-1*(*RNAi*) could

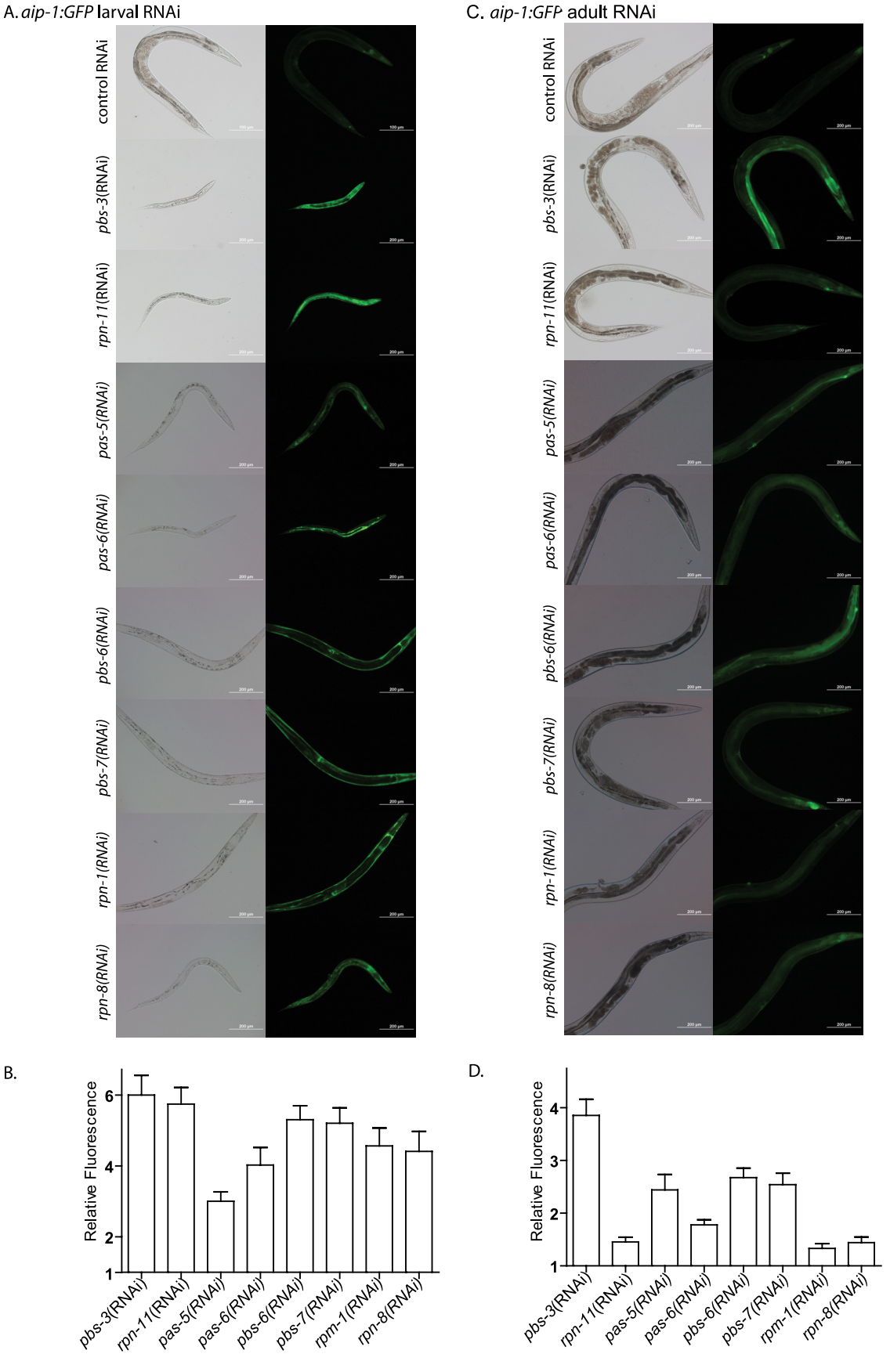
A. aip-1:GFP larval RNAi
control RNAi
pbs-3(RNAi)
rpn-11(RNAi)
pas-5(RNAi)
pas-6(RNAi)
pbs-6(RNAi)
pbs-7(RNAi)
rpn-1(RNAi)
rpn-8(RNAi)
C. aip-1:GFP adult RNAi
control RNAi
pbs-3(RNAi)
rpn-11(RNAi)
pas-5(RNAi)
pas-6(RNAi)
pbs-6(RNAi)
pbs-7(RNAi)
rpn-1(RNAi)
rpn-8(RNAi)
B.
Relative Fluorescence
1
2
4
6
pbs-3(RNAi)
rpn-11(RNAi)
pas-5(RNAi)
pas-6(RNAi)
pbs-6(RNAi)
pbs-7(RNAi)
rpm-1(RNAi)
rpn-8(RNAi)
D.
Relative Fluorescence
1
2
3
4
pbs-3(RNAi)
rpn-11(RNAi)
pas-5(RNAi)
pas-6(RNAi)
pbs-6(RNAi)
pbs-7(RNAi)
rpm-1(RNAi)
rpn-8(RNAi)

occur by different mechanisms. To test these possibilities, we asked whether the proteosomal dysfunction produced by *fah-1*(*RNAi*) has a mechanism in common with *hsp-1*(*RNAi*). First, we combined *fah-1*(*RNAi*) and *hsp-1*(*RNAi*) to see whether the combination would produce a further increase in *aip-1* expression. We found that the 1:1 combination of *fah-1*(*RNAi*) and *hsp-1*(*RNAi*) was not different than 1:1 *hsp-1*(*RNAi*) and control interfering RNA with regard to *aip-1p*:*GFP* expression (Fig. 12A and C). Second, we tested whether the activation of *aip-1p*:*GFP* requires *skn-1* by treating ALF127 with *hsp-1* interfering RNA. Similarly to *fah-1*(*RNAi*), we observed a reduction but not elimination of *aip-1* expression in the *skn-1*(−) progeny (Fig. 12B and D). Hence, the proteosomal dysfunction produced by *hsp-1*(*RNAi*) and that produced by *fah-1*(*RNAi*) likely share a response pathway.

DISCUSSION

***aip-1* expression is induced by tyrosine metabolites.** The AIRAP/*aip-1* genes play critical roles in the response to environmental arsenic exposure and are required for a normal worm life span (56, 57, 64). However, it was unknown if any endogenous sources of stress are recognized by this pathway. We found that metabolites which accumulate in worms with impaired tyrosine degradation due to RNAi against *fah-1* serve as a potent activator of *aip-1* expression (Fig. 2). Our results indicate that *aip-1* may not only be involved in facilitating the degradation of proteins that are either intrinsically unstable or damaged by external stressors but it could also be involved in preventing the accumulation of damaged proteins from chronic internal metabolic stress.

Similarly to arsenic, which is a known inducer of *aip-1* expression, the tyrosine metabolites maleylacetoacetate and fumarylacetoacetate produce multiple types of cell stress in exposed cells (7, 13, 15, 18, 21, 27–29, 36, 56, 59). The production of multiple types of cell stress simultaneously may distinguish inducers of *aip-1* expression from other exposures, like heat, peroxide, or tunicamycin, which stress cells but do not consistently activate *aip-1* expression (25, 56). While the exact mechanisms leading to *aip-1* expression are unknown, perhaps either overloading of proteosome capacity or the resulting accumulation of polyubiquitinated proteins may be involved because we find that RNAi against heat shock proteins or proteosomal subunits triggers *aip-1* expression.

It is unknown if other metabolic intermediates activate this pathway, but it is reasonable to expect that other similarly reactive compounds would. For example, the neurotransmitter dopamine is derived from tyrosine and has similar chemical properties. *In vivo*, dopamine produces types of cell damage similar to those produced by the tyrosine metabolites because recent work has shown increases in oxidative stress and activation of the unfolded protein response following exposure (10, 14, 19, 20, 24, 58). Perhaps AIRAP could be activated following dopamine exposure and play a role in the prevention of damage to dopaminergic neurons. This would be consistent with the observation that dopamine and proteosome inhibitors show synergistic effects with regard to cell toxicity and protein aggregation (47, 63, 65, 67).

Beyond other metabolic pathways, our results lead to the important conclusion that a large number of stressors which produce sufficient levels of proteotoxic stress can serve as inducers of *aip-1* expression. Hence, *aip-1*/AIRAP may be important in a significant number of disease states.

***aip-1* induction involves *skn-1*-dependent and -independent pathways.** The expression of *aip-1* is complex, as both *skn-1* and other transcription factors are required for full induction following exposure to tyrosine metabolites (Fig. 3 and 8). *skn-1* is the *C. elegans* homolog of the gene for Nrf2 and is directly activated by oxidative stress via multiple protein kinases and also via proteosomal dysfunction (2, 3, 26, 30, 33). Both arsenic and tyrosine metabolites could activate *skn-1* via either mechanism, as both oxidative stress and proteosomal dysfunction are observed following exposure to either stressor (18, 56, 57). Our results suggest only a modest role for the *sek-1* kinase pathway, as mutation of *pmk-1* only slightly reduces the induction of *aip-1* following exposure to tyrosine metabolites (Fig. 6). Recently, other kinases involved in the regulation of *skn-1* have been described, so these could represent an alternative way of stimulating *skn-1* activity (33). However, *skn-1* is not sufficient to activate the expression of *aip-1*, as genetic activation of *skn-1* with *wdr-23*(*RNAi*) results in only a marginal increase in expression (Fig. 7). Our findings are consistent with a model whereby both *skn-1* and other proteins, including *hsf-1*, bind to the *aip-1* promoter and direct expression (Fig. 13). Besides *hsf-1*, we have found evidence for additional transcription factors in the regulation of *aip-1* expression, and the recently described *slr-2* gene might also be directly involved in expression (data not shown) (35). These proteins may interact with *skn-1* either at the level of DNA binding or in the recruitment of coactivators or the basal transcription machinery.

Beyond regulating the *aip-1* promoter, *skn-1*, *hsf-1*, and perhaps additional transcription factors play an important role in cellular physiology. In addition to the activation of *aip-1*, RNAi against *hsp-1* and multiple proteosomal subunits also activates the expression of *gpdh-1*, which encodes glycerol-3-phosphate dehydrogenase and synthesizes intracellular glycerol in response to hypertonic stress (38). This suggests that the activated transcription factors could be involved in the regulation of responses to distinct stresses that have related cellular effects, such as an increase in protein aggregation (12). Importantly, while the cell damage and cell stress pathways show

FIG. 10. Proteosomal dysfunction induces *aip-1* expression. (A) Digital images of *aip-1p*:*GFP* worms treated with control interfering RNA or interfering RNA against proteosomal subunits starting at egg hatching. Many of these RNAi treatments also result in developmental arrest during larval life. (B) Graph of fluorescence measured from digital images ($n = 15$ for all; $P < 0.0001$ for all versus control interfering RNA). (C) Digital images of *aip-1p*:*GFP* worms treated with control interfering RNA or interfering RNA against proteosomal subunits starting at adulthood. (D) Graph of fluorescence measured from digital images [$n > 14$ for all; $P < 0.0001$ for *pbs*-3, *pas-6*, *pbs-6*, and *pbs-7*(*RNAi*) versus control interfering RNA, $P = 0.0029$ for *rpn-1*(*RNAi*) versus the control, $P = 0.0007$ for *rpn-8*(*RNAi*) versus the control, and $P = 0.0001$ for *pas-5* and *rpn-11*(*RNAi*) versus the control].

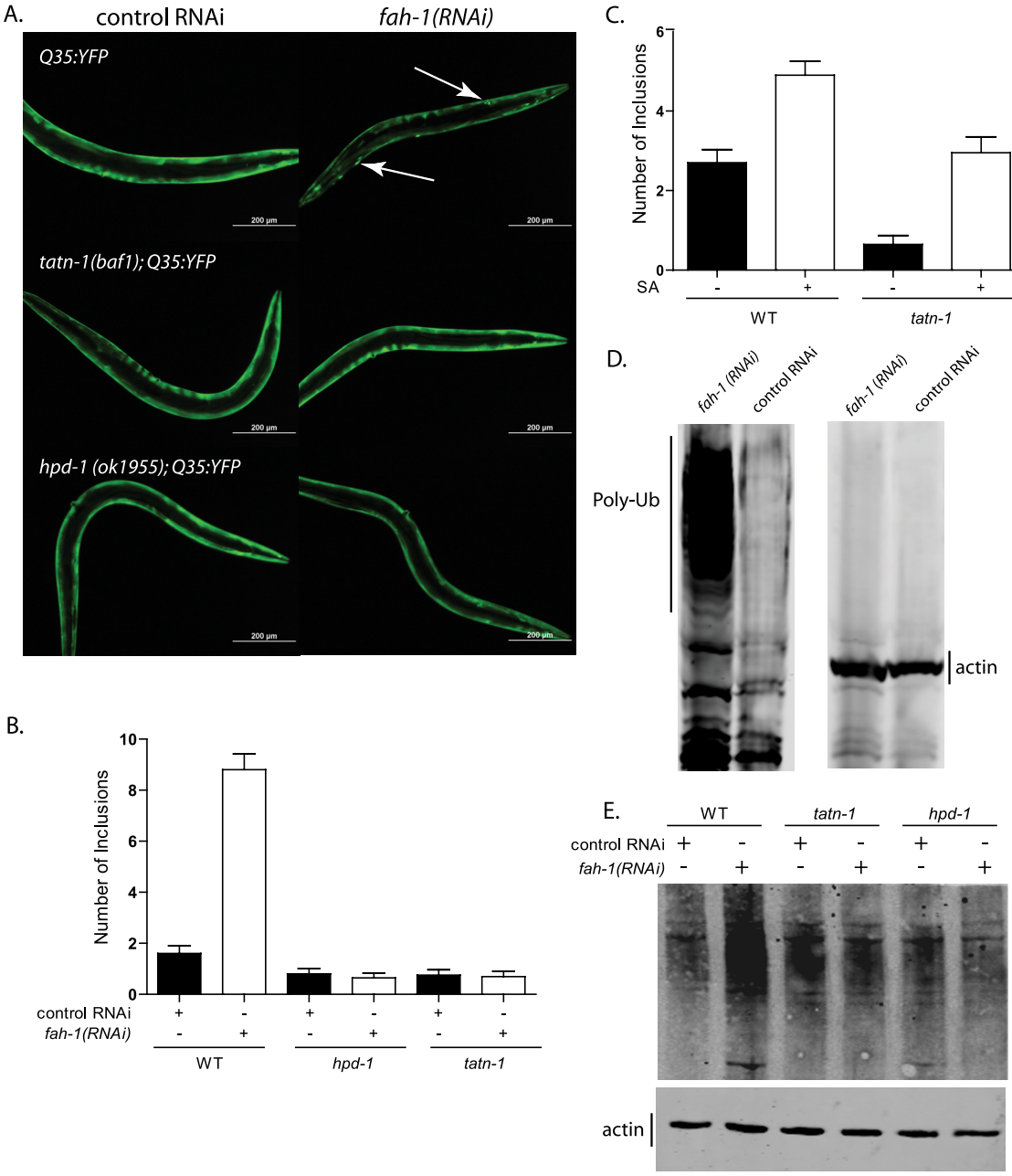

FIG. 11. Tyrosine metabolites produce proteosome dysfunction. (A) Images showing effects of control and *fah-1*(*RNAi*) treatments of AM140 (*Q35*:*YFP*) transgenic worms or *tatn-1* or *hpd-1* mutants carrying the *Q35*:*YFP* transgene. The arrows indicate aggregates in a *fah-1*(*RNAi*)-treated worm. (B) Graphical representation of aggregate counts from worms as shown in panel A [$n = 20$ for all groups; $P < 0.0001$ for wild-type (WT) *fah-1* versus WT control interfering RNA, $P = 0.595$ for *hpd-1*(*ok1955*) *fah-1* versus *hpd-1*(*ok1955*) control interfering RNA, $P = 0.868$ for *tatn-1*(*baf1*) *fah-1* versus *tatn-1*(*baf1*) control interfering RNA]. (C) Graph showing aggregate counts from *Q35*:*YFP* wild-type or *tatn-1* mutant transgenic worms treated with the tyrosine metabolite SA [$n = 20$ for all groups; $P < 0.0001$ for WT SA versus control treatment and for *tatn-1*(*baf1*) SA treatment versus control treatment]. (D) Total protein from *fah-1*- or control interfering RNA-treated TJ1060 worms was separated by SDS-PAGE and transferred to nitrocellulose. Blots were probed with an antiubiquitin antibody (left panel) or an antiactin antibody to demonstrate equal loading (right panel). (E) Total protein from N2, ALF103 [*tatn-1*(*baf1*)], and ALF114 [*hpd-19*(*ok1955*)] worms was separated by SDS-PAGE and transferred to nitrocellulose. Blots were probed with an antiubiquitin antibody (top) or an antiactin antibody to demonstrate equal loading (bottom).

some overlap, the outputs are rather distinct, which implies that somewhere in the process specificity with regard to stress and response is generated. For example, we find that exposure to osmotic stress does not have a significant effect on *aip-1* expression (Fig. 9). Perhaps the involvement of multiple transcription factors in the transcriptional response to stress allows tuning of the response to the character of a given stressor. For instance, the *aip-1* promoter contains binding sites for *skn-1*, whereas the *gpdh-1* promoter does not (Fisher, unpublished). This could suggest that inducers of *aip-1*, such as juglone,

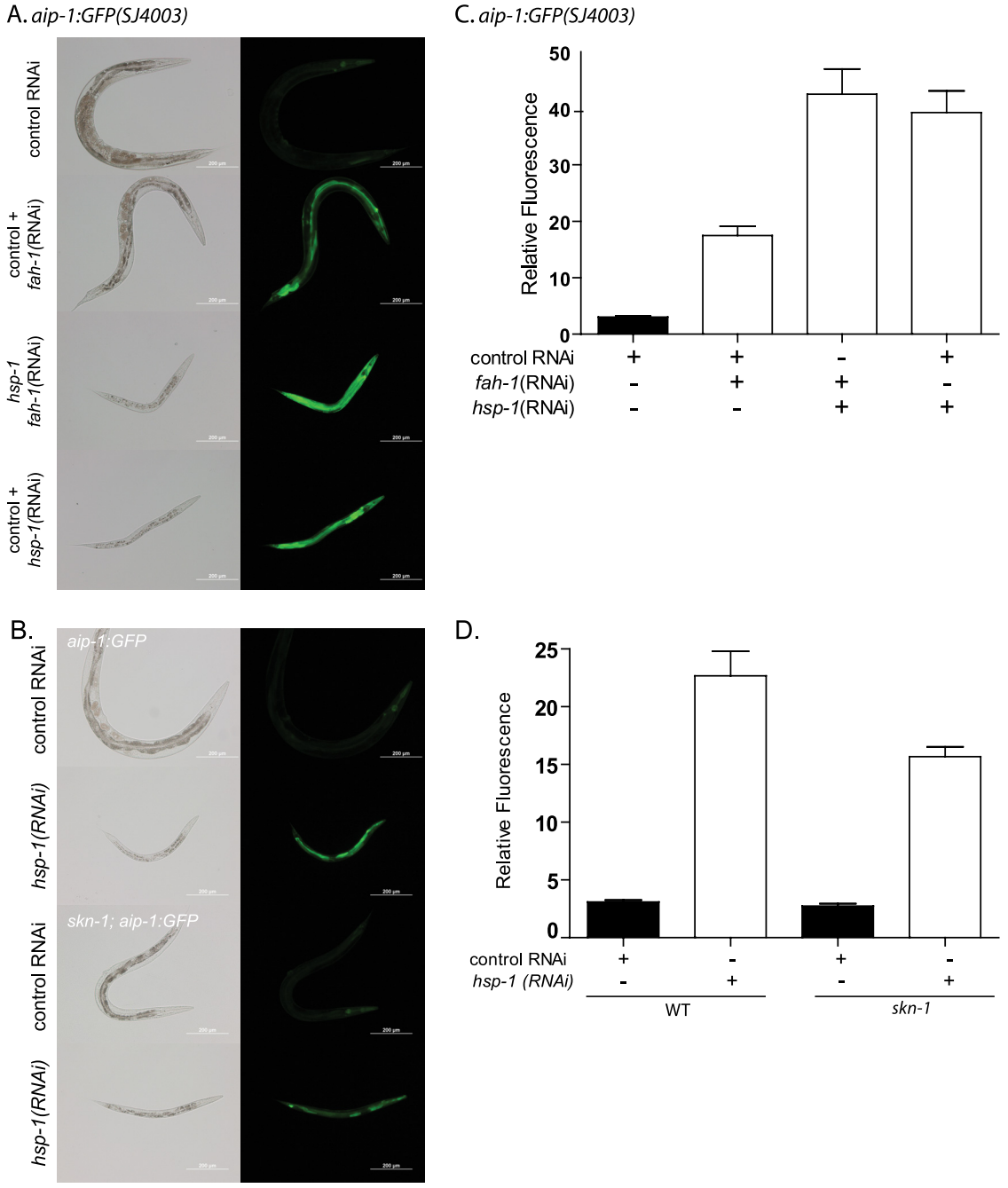

FIG. 12. Proteosomal dysfunction produced by *fah-1*(*RNAi*) and that produced by *hsp-1*(*RNAi*) trigger similar pathways. (A) Digital images of *aip-1p*:*GFP* worms treated with control interfering RNA, a 1:1 mixture of the control and *fah-1*(*RNAi*), a 1:1 mixture of *fah-1* and *hsp-1*(*RNAi*), or a 1:1 mixture of control interfering RNA and *hsp-1*(*RNAi*). *hsp-1*(*RNAi*) produces developmental arrest during larval life. (B) Digital photos of SJ4003 or ALF127 {*skn-1*(*zu135*)/*nT1*[*qIs51*] *aip-1p*:*GFP*} worms treated with the control or *hsp-1*(*RNAi*) from egg hatching. (C) Graph of fluorescence measured from the digital images in panel A [$n > 15$ for all; $P < 0.0001$ for all versus control interfering RNA, $P = 0.293$ for *hsp-1* and *fah-1*(*RNAi*) versus *hsp-1* and control interfering RNA]. (D) Graph of fluorescence measured from digital images in panel B [$n > 15$ for all; $P < 0.0001$ for *hsp-1* versus control interfering RNA for wild-type (WT) and *skn-1* and $P = 0.0034$ for wild-type *hsp-1*(*RNAi*) versus *skn-1* *hsp-1*(*RNAi*)].

arsenic, and tyrosine metabolites, need to have the ability to produce oxidative stress, whereas perhaps osmotic stress, which induces *gpdh-1*, does not and activates transcription factors other than *skn-1*. Further work is necessary to understand the molecular basis of the observed specificity.

Could AIRAP/aip-1 be a target of drug discovery? The AIRAP/*aip-1* pathway holds significant promise as a means to treat diseases associated with misfolded proteins in either the cytoplasm or the ER. This includes multiple neurodegenerative diseases, including those associated with polyglutamine repeat

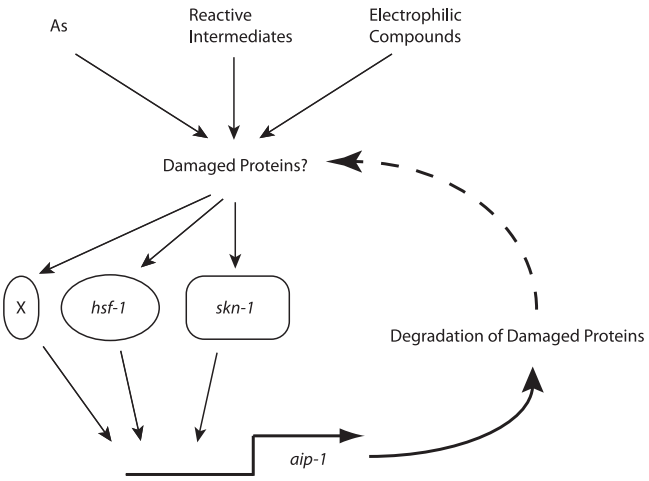

FIG. 13. Model of control of *aip-1* expression. Internal or external stressors such as arsenic, tyrosine metabolites, or juglone lead to the accumulation of damaged proteins due to relative proteosome dysfunction. Either proteosome dysfunction or oxidative stress related to the initial exposure leads to the activation of *skn-1*, which directly regulates *aip-1* expression. Secondary pathways, including *hsf-1* and perhaps others, marked X, are also activated and are required for *aip-1* expression. The production of AIP-1 protein then facilitates the degradation of the damaged proteins and might lead to termination of the initial trigger for *aip-1* induction.

expansion, Lewy bodies or Pick bodies (i.e., Parkinson's disease, Pick's disease, and dementia with Lewy bodies), some familial forms of amyotrophic lateral sclerosis, genetic diseases such as α1-antitrypsin deficiency associated with the accumulation of misfolded ER proteins, and metabolic diseases such as diabetes (54). Diabetes is particularly promising, as ER stress has been shown to lead to disease development in transgenic animals, and reduction of ER stress with chemical chaperones has treated diabetes in obese *ob*/*ob* mice (22, 51).

Furthermore, consumption of arsenic in drinking water has been associated with the development of diabetes, which is interesting in light of the production of several types of protein damage and induction of AIRAP/*aip-1* by arsenic exposure in worms and cultured cells (48). Finally, in worms, loss of *aip-1* has been shown to lead to premature aging (64). Hence, the development of compounds that can activate this cell stress response pathway without the production of cellular damage holds great potential for providing new opportunities to treat or, more importantly, prevent diseases associated with aging. This is consistent with recent work showing that increased *aip-1* expression can ameliorate the formation of amyloid in a worm model of Alzheimer's disease involving the expression of an Aβ peptide in muscle cells (23).

ACKNOWLEDGMENTS

We thank David Ron for the gift of the SJ4003 strain, and we thank the Caenorhabditis Genetics Center (which is funded by the NIH National Center for Research Resources) for worm strains. We also thank members of the Fisher lab and the Silverman lab, Clifford Luke, and Jeff Brodsky for comments and suggestions. We also thank anonymous reviewer 2 for the suggestion to test *hsf-1*.

This work was funded by NIH grant (AG028977) to A.L.F.

REFERENCES

1. **Abramoff, M. D., P. J. Magelhaes, and S. J. Ram.** 2004. Image processing with ImageJ. Biophotonics Int. **11:**36–42.
2. **An, J. H., and T. K. Blackwell.** 2003. SKN-1 links C. elegans mesendodermal specification to a conserved oxidative stress response. Genes Dev. **17:**1882–1893.
3. **An, J. H., K. Vranas, M. Lucke, H. Inoue, N. Hisamoto, K. Matsumoto, and T. K. Blackwell.** 2005. Regulation of the Caenorhabditis elegans oxidative stress defense protein SKN-1 by glycogen synthase kinase-3. Proc. Natl. Acad. Sci. U. S. A. **102:**16275–16280.
4. **Aponte, J. L., G. A. Sega, L. J. Hauser, M. S. Dhar, C. M. Withrow, D. A. Carpenter, E. M. Rinchik, C. T. Culiat, and D. K. Johnson.** 2001. Point mutations in the murine fumarylacetoacetate hydrolase gene: animal models for the human genetic disorder hereditary tyrosinemia type 1. Proc. Natl. Acad. Sci. U. S. A. **98:**641–645.
5. **Berezikov, E., C. I. Bargmann, and R. H. Plasterk.** 2004. Homologous gene targeting in Caenorhabditis elegans by biolistic transformation. Nucleic Acids Res. **32:**e40.
6. **Bergeron, A., M. D'Astous, D. E. Timm, and R. M. Tanguay.** 2001. Structural and functional analysis of missense mutations in fumarylacetoacetate hydrolase, the gene deficient in hereditary tyrosinemia type 1. J. Biol. Chem. **276:**15225–15231.
7. **Bergeron, A., R. Jorquera, D. Orejuela, and R. M. Tanguay.** 2006. Involvement of endoplasmic reticulum stress in hereditary tyrosinemia type I. J. Biol. Chem. **281:**5329–5334.
8. **Bishop, N. A., and L. Guarente.** 2007. Two neurons mediate diet-restriction-induced longevity in C. elegans. Nature **447:**545–549.
9. **Calfon, M., H. Zeng, F. Urano, J. H. Till, S. R. Hubbard, H. P. Harding, S. G. Clark, and D. Ron.** 2002. IRE1 couples endoplasmic reticulum load to secretory capacity by processing the XBP-1 mRNA. Nature **415:**92–96.
10. **Chen, L., Y. Ding, B. Cagniard, A. D. Van Laar, A. Mortimer, W. Chi, T. G. Hastings, U. J. Kang, and X. Zhuang.** 2008. Unregulated cytosolic dopamine causes neurodegeneration associated with oxidative stress in mice. J. Neurosci. **28:**425–433.
11. **Choe, K. P., A. J. Przybysz, and K. Strange.** 2009. The WD40 repeat protein WDR-23 functions with the CUL4/DDB1 ubiquitin ligase to regulate nuclear abundance and activity of SKN-1 in *Caenorhabditis elegans*. Mol. Cell. Biol. **29:**2704–2715.
12. **Choe, K. P., and K. Strange.** 2008. Genome-wide RNAi screen and in vivo protein aggregation reporters identify degradation of damaged proteins as an essential hypertonic stress response. Am. J. Physiol. Cell Physiol. **295:**C1488–C1498.
13. **Dieter, M. Z., S. L. Freshwater, M. L. Miller, H. G. Shertzer, T. P. Dalton, and D. W. Nebert.** 2003. Pharmacological rescue of the 14CoS/14CoS mouse: hepatocyte apoptosis is likely caused by endogenous oxidative stress. Free Radic. Biol. Med. **35:**351–367.
14. **Dukes, A. A., V. S. Van Laar, M. Cascio, and T. G. Hastings.** 2008. Changes in endoplasmic reticulum stress proteins and aldolase A in cells exposed to dopamine. J. Neurochem. **106:**333–346.
15. **Endo, F., S. Kubo, H. Awata, K. Kiwaki, H. Katoh, Y. Kanegae, I. Saito, J. Miyazaki, T. Yamamoto, C. Jakobs, S. Hattori, and I. Matsuda.** 1997. Complete rescue of lethal albino c14CoS mice by null mutation of 4-hydroxyphenylpyruvate dioxygenase and induction of apoptosis of hepatocytes in these mice by in vivo retrieval of the tyrosine catabolic pathway. J. Biol. Chem. **272:**24426–24432.
16. **Ferguson, A. A., and A. L. Fisher.** 2009. Retrofitting ampicillin resistant vectors by recombination for use in generating C. elegans transgenic animals by bombardment. Plasmid **62:**140–145.
17. **Fernández-Cañón, J. M., and M. A. Penalva.** 1995. Fungal metabolic model for human type I hereditary tyrosinaemia. Proc. Natl. Acad. Sci. U. S. A. **92:**9132–9136.
18. **Fisher, A. L., K. E. Page, G. J. Lithgow, and L. Nash.** 2008. The Caenorhabditis elegans K10C2.4 gene encodes a member of the fumarylacetoacetate hydrolase family: a Caenorhabditis elegans model of type I tyrosinemia. J. Biol. Chem. **283:**9127–9135.
19. **Graham, D. G.** 1978. Oxidative pathways for catecholamines in the genesis of neuromelanin and cytotoxic quinones. Mol. Pharmacol. **14:**633–643.
20. **Graham, D. G., S. M. Tiffany, W. R. Bell, Jr., and W. F. Gutknecht.** 1978. Autoxidation versus covalent binding of quinones as the mechanism of toxicity of dopamine, 6-hydroxydopamine, and related compounds toward C1300 neuroblastoma cells in vitro. Mol. Pharmacol. **14:**644–653.
21. **Grompe, M., M. al-Dhalimy, M. Finegold, C. N. Ou, T. Burlingame, N. G. Kennaway, and P. Soriano.** 1993. Loss of fumarylacetoacetate hydrolase is responsible for the neonatal hepatic dysfunction phenotype of lethal albino mice. Genes Dev. **7:**2298–2307.
22. **Harding, H. P., H. Zeng, Y. Zhang, R. Jungries, P. Chung, H. Plesken, D. D. Sabatini, and D. Ron.** 2001. Diabetes mellitus and exocrine pancreatic dysfunction in perk−/− mice reveals a role for translational control in secretory cell survival. Mol. Cell **7:**1153–1163.
23. **Hassan, W. M., D. A. Merin, V. Fonte, and C. D. Link.** 2009. AIP-1 amelio-

rates beta-amyloid peptide toxicity in a Caenorhabditis elegans Alzheimer's disease model. Hum. Mol. Genet. **18:**2739–2747.
24. **Hastings, T. G., D. A. Lewis, and M. J. Zigmond.** 1996. Role of oxidation in the neurotoxic effects of intrastriatal dopamine injections. Proc. Natl. Acad. Sci. U. S. A. **93:**1956–1961.
25. **Hsu, A. L., C. T. Murphy, and C. Kenyon.** 2003. Regulation of aging and age-related disease by DAF-16 and heat-shock factor. Science **300:**1142–1145.
26. **Inoue, H., N. Hisamoto, J. H. An, R. P. Oliveira, E. Nishida, T. K. Blackwell, and K. Matsumoto.** 2005. The C. elegans p38 MAPK pathway regulates nuclear localization of the transcription factor SKN-1 in oxidative stress response. Genes Dev. **19:**2278–2283.
27. **Jorquera, R., and R. M. Tanguay.** 1999. Cyclin B-dependent kinase and caspase-1 activation precedes mitochondrial dysfunction in fumarylacetoacetate-induced apoptosis. FASEB J. **13:**2284–2298.
28. **Jorquera, R., and R. M. Tanguay.** 2001. Fumarylacetoacetate, the metabolite accumulating in hereditary tyrosinemia, activates the ERK pathway and induces mitotic abnormalities and genomic instability. Hum. Mol. Genet. **10:**1741–1752.
29. **Jorquera, R., and R. M. Tanguay.** 1997. The mutagenicity of the tyrosine metabolite, fumarylacetoacetate, is enhanced by glutathione depletion. Biochem. Biophys. Res. Commun. **232:**42–48.
30. **Kahn, N. W., S. L. Rea, S. Moyle, A. Kell, and T. E. Johnson.** 2008. Proteasomal dysfunction activates the transcription factor SKN-1 and produces a selective oxidative-stress response in Caenorhabditis elegans. Biochem. J. **409:**205–213.
31. **Kamath, R. S., and J. Ahringer.** 2003. Genome-wide RNAi screening in Caenorhabditis elegans. Methods **30:**313–321.
32. **Kapulkin, W. J., B. G. Hiester, and C. D. Link.** 2005. Compensatory regulation among ER chaperones in C. elegans. FEBS Lett. **579:**3063–3068.
33. **Kell, A., N. Ventura, N. Kahn, and T. E. Johnson.** 2007. Activation of SKN-1 by novel kinases in Caenorhabditis elegans. Free Radic. Biol. Med. **43:**1560–1566.
34. **Kelsey, G., S. Ruppert, F. Beermann, C. Grund, R. M. Tanguay, and G. Schutz.** 1993. Rescue of mice homozygous for lethal albino deletions: implications for an animal model for the human liver disease tyrosinemia type 1. Genes Dev. **7:**2285–2297.
35. **Kirienko, N. V., and D. S. Fay.** 2010. SLR-2 and JMJC-1 regulate an evolutionarily conserved stress-response network. EMBO J. **29:**727–739.
36. **Laberge, C., A. Lescault, and R. M. Tanguay.** 1986. Hereditary tyrosinemias (type I): a new vista on tyrosine toxicity and cancer. Adv. Exp. Med. Biol. **206:**209–221.
37. **Lamitina, S. T., R. Morrison, G. W. Moeckel, and K. Strange.** 2004. Adaptation of the nematode Caenorhabditis elegans to extreme osmotic stress. Am. J. Physiol. Cell Physiol. **286:**C785–C791.
38. **Lamitina, T., C. G. Huang, and K. Strange.** 2006. Genome-wide RNAi screening identifies protein damage as a regulator of osmoprotective gene expression. Proc. Natl. Acad. Sci. U. S. A. **103:**12173–12178.
39. **Lindblad, B., S. Lindstedt, and G. Steen.** 1977. On the enzymic defects in hereditary tyrosinemia. Proc. Natl. Acad. Sci. U. S. A. **74:**4641–4645.
40. **Link, C. D., and C. J. Johnson.** 2002. Reporter transgenes for study of oxidant stress in Caenorhabditis elegans. Methods Enzymol. **353:**497–505.
41. **Livak, K. J., and T. D. Schmittgen.** 2001. Analysis of relative gene expression data using real-time quantitative PCR and the 2(-Delta Delta C(T)) Method. Methods **25:**402–408.
42. **Marshall, O. J.** 2004. PerlPrimer: cross-platform, graphical primer design for standard, bisulphite and real-time PCR. Bioinformatics **20:**2471–2472.
43. **Mitchell, G. A., M. Grompe, M. Lambert, R. M. Tanguay, and C. R. Scriver.** 2001. Hypertyrosinemia, p. 1777–1805. *In* C. R. Scriver, A. L. Beaudet, W. S. Sly, D. Valle, B. Childs, K. W. Kinzler, and B. Vogelstein (ed.), The metabolic and molecular basis of inherited disease. McGraw-Hill, New York, NY.
44. **Moran, G. R.** 2005. 4-Hydroxyphenylpyruvate dioxygenase. Arch. Biochem. Biophys. **433:**117–128.
45. **Morley, J. F., H. R. Brignull, J. J. Weyers, and R. I. Morimoto.** 2002. The threshold for polyglutamine-expansion protein aggregation and cellular toxicity is dynamic and influenced by aging in Caenorhabditis elegans. Proc. Natl. Acad. Sci. U. S. A. **99:**10417–10422.
46. **Morley, J. F., and R. I. Morimoto.** 2004. Regulation of longevity in Caenorhabditis elegans by heat shock factor and molecular chaperones. Mol. Biol. Cell **15:**657–664.
47. **Mytilineou, C., K. S. McNaught, P. Shashidharan, J. Yabut, R. J. Baptiste, A. Parnandi, and C. W. Olanow.** 2004. Inhibition of proteasome activity sensitizes dopamine neurons to protein alterations and oxidative stress. J. Neural Transm. **111:**1237–1251.
48. **Navas-Acien, A., E. K. Silbergeld, R. Pastor-Barriuso, and E. Guallar.** 2008. Arsenic exposure and prevalence of type 2 diabetes in US adults. JAMA **300:**814–822.
49. **Nollen, E. A., S. M. Garcia, G. van Haaften, S. Kim, A. Chavez, R. I. Morimoto, and R. H. Plasterk.** 2004. Genome-wide RNA interference screen identifies previously undescribed regulators of polyglutamine aggregation. Proc. Natl. Acad. Sci. U. S. A. **101:**6403–6408.
50. **Oliveira, R. P., J. Porter Abate, K. Dilks, J. Landis, J. Ashraf, C. T. Murphy, and T. K. Blackwell.** 2009. Condition-adapted stress and longevity gene regulation by Caenorhabditis elegans SKN-1/Nrf. Aging Cell **8:**524–541.
51. **Ozcan, U., E. Yilmaz, L. Ozcan, M. Furuhashi, E. Vaillancourt, R. O. Smith, C. Z. Gorgun, and G. S. Hotamisligil.** 2006. Chemical chaperones reduce ER stress and restore glucose homeostasis in a mouse model of type 2 diabetes. Science **313:**1137–1140.
52. **Phaneuf, D., Y. Labelle, D. Berube, K. Arden, W. Cavenee, R. Gagne, and R. M. Tanguay.** 1991. Cloning and expression of the cDNA encoding human fumarylacetoacetate hydrolase, the enzyme deficient in hereditary tyrosinemia: assignment of the gene to chromosome 15. Am. J. Hum. Genet. **48:**525–535.
53. **Przybysz, A. J., K. P. Choe, L. J. Roberts, and K. Strange.** 2009. Increased age reduces DAF-16 and SKN-1 signaling and the hormetic response of Caenorhabditis elegans to the xenobiotic juglone. Mech. Ageing Dev. **130:**357–369.
54. **Schwartz, A. L., and A. Ciechanover.** 2009. Targeting proteins for destruction by the ubiquitin system: implications for human pathobiology. Annu. Rev. Pharmacol. Toxicol. **49:**73–96.
55. **Shostak, Y., M. R. Van Gilst, A. Antebi, and K. R. Yamamoto.** 2004. Identification of C. elegans DAF-12-binding sites, response elements, and target genes. Genes Dev. **18:**2529–2544.
56. **Sok, J., M. Calfon, J. Lu, P. Lichtlen, S. G. Clark, and D. Ron.** 2001. Arsenite-inducible RNA-associated protein (AIRAP) protects cells from arsenite toxicity. Cell Stress Chaperones **6:**6–15.
57. **Stanhill, A., C. M. Haynes, Y. Zhang, G. Min, M. C. Steele, J. Kalinina, E. Martinez, C. M. Pickart, X. P. Kong, and D. Ron.** 2006. An arsenite-inducible 19S regulatory particle-associated protein adapts proteasomes to proteotoxicity. Mol. Cell **23:**875–885.
58. **Stokes, A. H., T. G. Hastings, and K. E. Vrana.** 1999. Cytotoxic and genotoxic potential of dopamine. J. Neurosci. Res. **55:**659–665.
59. **Sun, M. S., S. Hattori, S. Kubo, H. Awata, I. Matsuda, and F. Endo.** 2000. A mouse model of renal tubular injury of tyrosinemia type 1: development of de Toni Fanconi syndrome and apoptosis of renal tubular cells in Fah/Hpd double mutant mice. J. Am. Soc. Nephrol. **11:**291–300.
60. **Tawe, W. N., M. L. Eschbach, R. D. Walter, and K. Henkle-Duhrsen.** 1998. Identification of stress-responsive genes in Caenorhabditis elegans using RT-PCR differential display. Nucleic Acids Res. **26:**1621–1627.
61. **Wang, X., B. Thomas, R. Sachdeva, L. Arterburn, L. Frye, P. G. Hatcher, D. G. Cornwell, and J. Ma.** 2006. Mechanism of arylating quinone toxicity involving Michael adduct formation and induction of endoplasmic reticulum stress. Proc. Natl. Acad. Sci. U. S. A. **103:**3604–3609.
62. **Yoneda, T., C. Benedetti, F. Urano, S. G. Clark, H. P. Harding, and D. Ron.** 2004. Compartment-specific perturbation of protein handling activates genes encoding mitochondrial chaperones. J. Cell Sci. **117:**4055–4066.
63. **Yoshimoto, Y., K. Nakaso, and K. Nakashima.** 2005. L-dopa and dopamine enhance the formation of aggregates under proteasome inhibition in PC12 cells. FEBS Lett. **579:**1197–1202.
64. **Yun, C., A. Stanhill, Y. Yang, Y. Zhang, C. M. Haynes, C. F. Xu, T. A. Neubert, A. Mor, M. R. Philips, and D. Ron.** 2008. Proteasomal adaptation to environmental stress links resistance to proteotoxicity with longevity in Caenorhabditis elegans. Proc. Natl. Acad. Sci. U. S. A. **105:**7094–7099.
65. **Zafar, K. S., S. H. Inayat-Hussain, and D. Ross.** 2007. A comparative study of proteasomal inhibition and apoptosis induced in N27 mesencephalic cells by dopamine and MG132. J. Neurochem. **102:**913–921.
66. **Zhang, Y., L. Nash, and A. L. Fisher.** 2008. A simplified, robust, and streamlined procedure for the production of C. elegans transgenes via recombineering. BMC Dev. Biol. **8:**119.
67. **Zhou, Z., S. Kerk, and T. Meng Lim.** 2008. Endogenous dopamine (DA) renders dopaminergic cells vulnerable to challenge of proteasome inhibitor MG132. Free Radic. Res. **42:**456–466.